J. Fluid Mech. (2004), *vol.* 505, *pp.* 123–151.
DOI: 10.1017/S0022112004008456 Printed in the United Kingdom

Similarity of decaying isotropic turbulence with a passive scalar

By R. A. ANTONIA[1] AND P. ORLANDI[2]

[1]Discipline of Mechanical Engineering, University of Newcastle, NSW, 2308, Australia

[2]Dipartimento di Meccanica e Aeronautica, Universita Degli Studi di Roma "La Sapienza", 00184 Rome, Italy

(Received 11 April 2003 and in revised form 11 November 2003)

Direct numerical simulations have been carried out for decaying homogeneous isotropic turbulence in a periodic box. Data for both the velocity and passive scalar fields are considered, the latter for several values of the Schmidt number Sc. The focus is on how the three-dimensional spectra $E(k,t)$ and $E_\theta(k,t)$ and the spectral transfer functions $T(k,t)$ and $T_\theta(k,t)$ satisfy similarity during decay. The evolution of these four quantities provides qualified support for the equilibrium similarity proposal of George (1992*a*, *b*). In particular, this proposal provides a reliable means of calculating the transfer functions, starting with known distributions of $E(k,t)$ and $E_\theta(k,t)$. However, at sufficiently large values of the wavenumber k, normalizations by Kolmogorov and Batchelor variables yield a better collapse of these quantities than the use of equilibrium similarity The distributions of $E_\theta(k,t)$ and $T_\theta(k,t)$ do not depend on Sc, when the latter is in the range $0.7 \leqslant Sc \leqslant 7$, irrespective of the normalization adopted. The velocity derivative skewness and mixed velocity–scalar derivative skewness approach constant values as t increases. This is in disagreement with equilibrium similarity but in accord with the observed high-wavenumber collapse of Kolmogorov and Batchelor normalized distributions of $E(k,t)$ and $E_\theta(k,t)$.

1. Introduction

Since the seminal paper by Kármán & Howarth (1938) significant attention has been given to how homogeneous isotropic turbulence (HIT) decays from an initially prescribed state. Most attempts (e.g. Dryden 1943; Batchelor 1948; Batchelor & Townsend 1948; Lin 1948; Kármán & Lin 1949; Goldstein 1951) have assumed from the outset that the same similarity scales apply to $E(k)$ and $T(k)$, the three-dimensional energy spectrum and energy spectral transfer function respectively, which appear in the well-known equation

$$\frac{\partial E(k,t)}{\partial t} = T(k,t) - 2\nu k^2 E(k,t), \tag{1}$$

where ν is the kinematic viscosity. George (1992*a*) showed that the possibility that the similarity scales for $E(k)$ and $T(k)$ may differ is admitted by (1). This allowed an important relaxation of the assumptions made previously by Kármán & Howarth and many subsequent investigators. Later, George (see Wang *et al.* 2000) made a formal distinction between the self-preserving hypothesis which relies on single length and velocity scales and the equilibrium hypothesis which allows the assumption of self-preservation to be relaxed and permits the appropriate similarity scales to

be determined from the governing equations. George found that the appropriate similarity scales admitted by (1) are the turbulent energy $\langle q^2(t)\rangle$, where

$$\langle q^2(t)\rangle/2 = \int_0^\infty E(k,t)\,\mathrm{d}k,$$

and the Taylor microscale $\lambda \equiv (5\langle q^2(t)\rangle/\langle\varepsilon(t)\rangle)^{1/2}$ where

$$\langle\varepsilon(t)\rangle \equiv 2\nu\int_0^\infty k^2 E(k,t)\,\mathrm{d}k$$

is the mean energy dissipation rate.

The energy $\langle q^2(t)\rangle$ can now exhibit a power-law decay behaviour, namely $\langle q^2(t)\rangle \sim (t-t_0)^m$ with $m \leqslant -1$, regardless of the magnitude of the Taylor microscale Reynolds number $R_\lambda = ((\langle q^2\rangle/3)^{1/2}\lambda/\nu)$. The attraction of this outcome is that similarity of decay should be achievable in both experiments and simulations, where m is typically smaller than -1 and R_λ is usually small and varies either with x or t. This is in contrast with the self-preserving arymptopic solution with $m=-1$ and an infinitely large and time-independent R_λ (e.g. Speziale & Bernard 1992).

George (1992*b*) also considered the equation governing the evolution of a scalar field (in his case, temperature) in HIT, namely

$$\frac{\partial E_\theta(k,t)}{\partial t} = T_\theta(k,t) - 2\nu_\theta k^2 E_\theta(k,t), \tag{2}$$

where $E_\theta(k,t)$ and $T_\theta(k,t)$ represent the spectrum and spectral transfer function respectively of the scalar fluctuation θ and ν_θ is the molecular diffusivity of the scalar. He found that (2) admits a similarity solution with the possibility of $E_\theta(k,t)$ and $T_\theta(k,t)$ having different scales. Like $\langle q^2(t)\rangle$, the scalar variance $\langle\theta^2(t)\rangle$ can decay according to a power-law behaviour, i.e. $\langle\theta^2(t)\rangle \sim (t-t_{\theta_0})^n$, where $n(\leqslant -1)$ and the virtual origin t_{θ_0} depend on the initial conditions. The appropriate similarity scales are $\langle\theta^2\rangle$ and the Corrsin microscale $\lambda_\theta \equiv (3\nu_\theta\langle\theta^2\rangle/\langle\varepsilon_\theta\rangle)^{1/2}$, where $\langle\varepsilon_\theta\rangle$ is the mean scalar dissipation rate of $\langle\theta^2\rangle/2$; note that

$$\langle\theta^2(t)\rangle = \int_0^\infty E_\theta(k,t)\,\mathrm{d}k, \quad \langle\varepsilon_\theta(t)\rangle = \nu_\theta\int_0^\infty k^2\,E_\theta(k,t)\,\mathrm{d}k.$$

Hereafter, the combined proposals in George (1992*a*) and George (1992*b*) will be referred to as G92.

Grid turbulence data have been extensively used to test similarity proposals for HIT. However, their major disadvantage is that they satisfy HIT only approximately, even when a contraction is added downstream of the grid (e.g. Comte-Bellot & Corrsin 1966). Another related disadvantage is that $E(k,t)$, $T(k,t)$ and the corresponding scalar counterparts $E_\theta(k,t)$ and $T_\theta(k,t)$ are not readily determinable from grid turbulence measurements.† Consequently, assumptions are required, especially for obtaining the spectral transfer functions (e.g. Uberoi 1963; Van Atta & Chen 1969; Yeh & Van Atta 1973, Helland, Van Atta & Stegen 1977). Direct numerical simulations (DNS) of decaying turbulence in a periodic box do not suffer from the previous disadvantages. They may, however, suffer from the box size effect and the possibility that the smallest flow scales are not resolved adequately (grid turbulence experiments are not immune from these effects). Although active grids

† This difficulty can be circumvented in physical space by considering the energy structure equation (Antonia *et al.* 2003).

(e.g. Mydlarski & Warhaft 1996, 1999) offer the possibility of achieving values of R_λ of the order of 1000, this does not seem to have been exploited in the context of testing the form of similarity during decay. Comparable values of R_λ have recently been obtained in DNSs (e.g. Gotoh, Fukayama & Nakano 2002; Kaneda *et al.* 2003), of HIT but it should be made clear that there are for 'forced' turbulence, a much less demanding situation than considered in this paper.

To date, there has only been limited verification of the equilibrium similarity hypothesis for the passive scalar field. For the thermal grid turbulence data of Warhaft & Lumley (1978), the Prandtl number Pr or, more generally, the Schmidt number $Sc\,(\equiv\nu/\nu_\theta)$ was about 0.7, temperature being introduced via an electrically heated mandoline downstream of the grid. In the present paper, we analyse DNS data obtained for decaying turbulence inside a periodic box at several values of Sc (0.7, 1, 3, 7, 15) and small $R_\lambda\,(\lesssim 40)$. The velocity field is the same in each case and the same scalar spectrum was assumed at $t = 0$ for each value of Sc. The main objective is to examine how closely $E(k,t)$, $E_\theta(k,t)$, $T(k,t)$, $T_\theta(k,t)$ satisfy equilibrium similarity. However, we also assess the appropriateness of using either Kolmogorov scaling or Batchelor scaling to normalize these four spectral quantities. The small values of R_λ allow the high-wavenumber end of the velocity and scalar spectra (albeit for Sc not much greater than 1) to be resolved more accurately than has been possible hitherto, thus allowing scaling with Kolmogorov and/or Batchelor variables to be compared critically against G92. It is widely accepted that Kolmogorov scaling applies strictly when R_λ is large, the wavenumbers are high and any effect from large-scale inhomogeneities is small, if not negligible. The assumptions which underpin the similarity hypotheses of Kolmogorov (1941) and their later modifications (Kolmogorov 1962) are therefore likely to be satisfied asymtopically, under homogeneous isotropic conditions. For decaying HIT with $m = -1$ (and $R_\lambda \to \infty$), the equilibrium similarity hypothesis is completely consistent with similarity based on Kolmogorov variables. There is nonetheless a significant body of evidence (e.g. Kim & Antonia 1993; Nelkin 1994) which supports this similarity for sufficiently small scales even when R_λ is small, provided extraneous effects, such as that due to the mean shear, are small. It is therefore important to compare Kolmogorov scaling with equilibrium similarity scaling in a flow where R_λ is small and varies with time. Equally, in the case of the scalar, it is of interest to check the inter-relationship between equilibrium similarity and a scaling based on Batchelor variables, in the light of relatively recent DNS data which indicate that, at sufficiently large wavenumbers, the scalar spectrum, especially when $Sc \gtrsim 1$, scales on Batchelor variables (e.g. Kerr 1990; Bogucki, Domaradski & Yeung 1997; Brethouwer & Niewstadt 1999; Orlandi & Antonia 2002; Yeung, Xu & Sreenivasan; the reader should consult the review of Antonia & Orlandi 2003*a* for other references).

2. Numerical details

The present DNS scheme uses an energy conservative finite difference (FD) code (240^3 grid), which is second-order in space and time and is applied to a cubic box of size 2π. The FD scheme has been described in Orlandi (1999) where results obtained with this scheme are compared with those obtained with the pseudospectral (PS) scheme. Satisfactory agreement has been found (Orlandi & Antonia 2002) between spectra obtained by the two methods but, as will be shown in § 6, the FD approach avoids the problem of truncation in Fourier space, i.e. that energy that should be transferred to higher wavenumbers (than those resolved) piles up at the highest

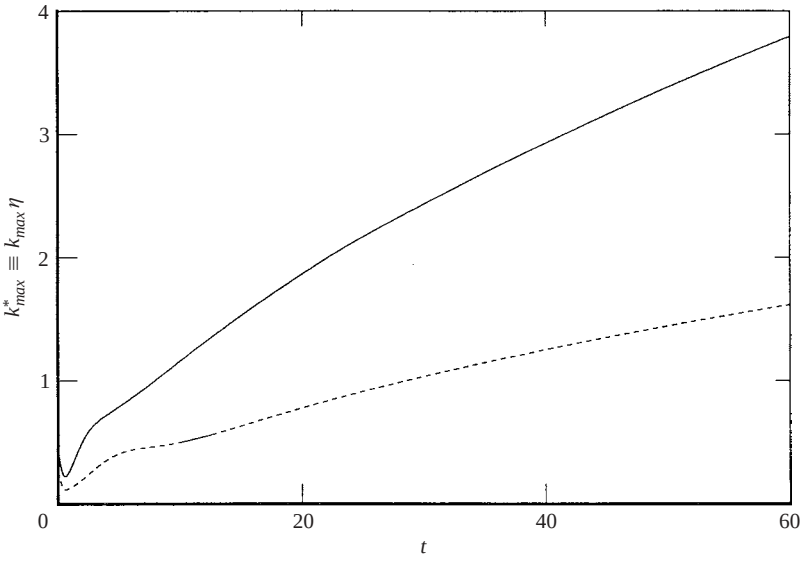

FIGURE 1. Dependence on t of the maximum wavenumber of the simulation, normalized by the Kolmogorov length scale η: —, lower Reynolds number simulation (240^3); – – –, higher Reynolds number simulation (270^3).

wavenumber (see Wang *et al.* 2000). A particular distribution of $E(k, t)$ was prescribed at $t = 0$, as in Mansour & Wray (1994), namely

$$E(k,0) = \frac{\langle q^2 \rangle}{2A} \frac{k^\sigma}{k_p^{\sigma+1}} \exp\left[-\frac{\sigma}{2}\left(\frac{k}{k_p}\right)^2\right],$$

where k_p is the wavenumber at which $E(k, 0)$ is maximum, σ is a parameter (here set equal to 4) related to the low-wavenumber behaviour and

$$A \equiv \int_0^\infty k^\sigma \exp(-\sigma k^2)\,\mathrm{d}k.$$

A parametric study of the effect of k_p indicated that the magnitude of k_p did not affect the power-law decay rate of the mean energy; increasing k_p resulted in different types of transients and in the decay occurring at an earlier time. de Bruyn Kops & Riley (1998) suggested that $k_{min}L$ should be less than 0.3 in order to ensure negligible energy transfer from the lowest wavenumbers (k_{min} is the lowest wavenumber and L is the integral length scale, defined in § 6). For the present 240^3 simulation, $k_{min}L$ is 0.29 at $t = 0$, compared with 0.23 for the Wray (1998) simulation. As t increases, L becomes more difficult to determine accurately since the lowest wavenumbers are less well resolved. Our main interest is, however, in the behaviour of the small scales. In this context, figure 1 shows that for the 240^3 simulation, $k_{max}\eta$ (k_{max} is the maximum wavenumber and $\eta \equiv \nu^{3/4}\langle\varepsilon\rangle^{-1/4}$ is the Kolmogorov microscale) is in the range 1 to 4 when $10 \leqslant t \leqslant 60$, the range of interest here (see § 3). We have also included the distribution of $k_{max}\eta$ obtained with a 270^3 grid. For this simulation, R_λ is about 50% larger over the range $10 \leqslant t \leqslant 60$ than for the other simulation but the small-scale resolution is clearly poorer. Unless otherwise indicated, all results presented here are for the 240^3 simulation. As in the simulation of Wray, t has been made dimensionless using arbitrary velocity (at $t = 0$, $\int_0^\infty E(k)\mathrm{d}k = 3/2$) and length (box size 2π) scales.

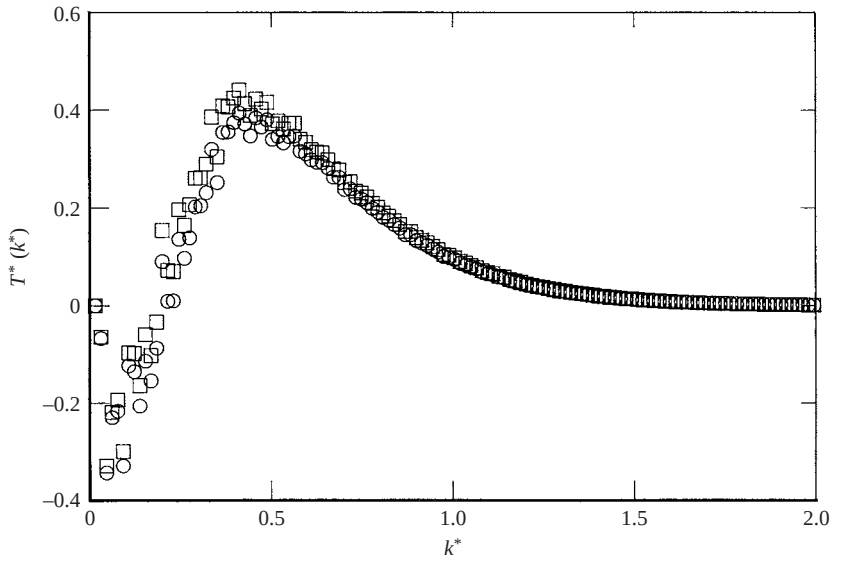

FIGURE 2. Comparison between the directly evaluated distribution of $T(k)$ and that calculated from the spectral energy equation. DNS data of Wray (1998). ○, Direct estimate; □, calculated indirectly using the spectral energy equation.

For the scalar, the simulation was started with a random phase spectrum, the prescription for $E_\theta(k, 0)$ being similar to that for $E(k, 0)$. In particular, the same distribution of $E_\theta(k, 0)$ was adopted for each of the five chosen values (0.7, 1, 3, 7, 15) for Sc.

The transfer functions $T(k, t)$ and $T_\theta(k, t)$ have been computed indirectly using (1) and (2), i.e.

$$T(k,t) = \frac{\partial E(k,t)}{\partial t} + 2\nu k^2 E(k,t)$$

and

$$T_\theta(k,t) = \frac{\partial E_\theta(k,t)}{\partial t} + 2\nu_\theta k^2 E_\theta(k,t).$$

We have verified, however, (figure 2) that the indirect calculation of $T(k, t)$ is in close agreement with that obtained directly from the triadic interactions in wavenumber space (see e.g. Domaradzki & Rogallo 1990) using the DNS database of Wray (1998).

3. Power–law decay of $\langle q^2 \rangle$ and $\langle \theta^2 \rangle$

Since some time is required before the effect of the starting transients in the simulation disappears, it is of interest to first examine the time histories of quantities such as $\langle q^2(t) \rangle$ and $\langle \varepsilon(t) \rangle$. These are plotted in log–log coordinates in figure 3. The mean energy $\langle q^2(t) \rangle$ remains approximately constant at the start of the simulation before decreasing relatively sharply for $t \geqslant 0.5$. There is a subsequent slower decrease which starts at $t \approx 2$. This is followed by another transition ($t \geqslant 10$) to a further power-law decay behaviour up to the end ($t = 60$) of the simulation. For $t \geqslant 0.5$, $\langle \varepsilon(t) \rangle$ behaves in a similar manner to $\langle q^2(t) \rangle$. There is, however, a rise in $\langle \varepsilon(t) \rangle$ at small t. Corresponding to the maximum at $t = 0.6$ is a minimum for both λ^2 and R_λ. Note

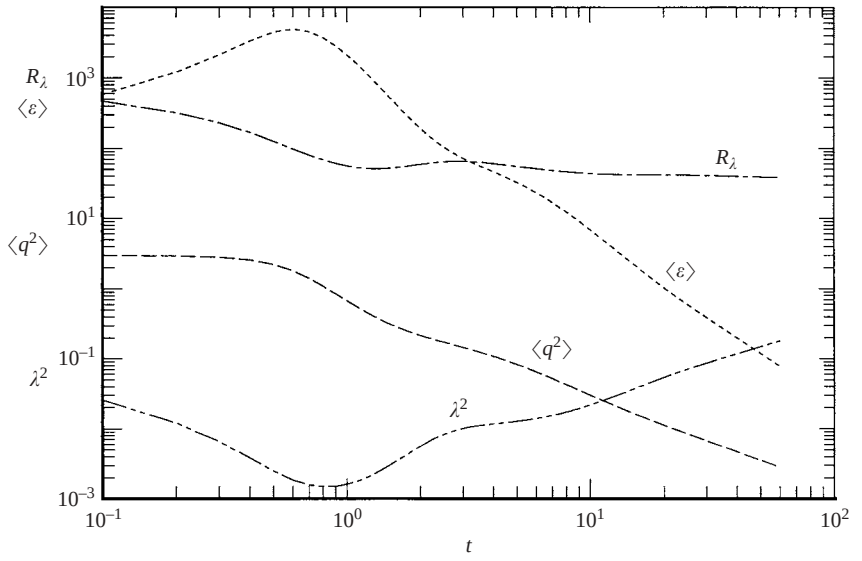

FIGURE 3. Temporal histories of $\langle q^2\rangle$, $\langle\varepsilon\rangle$, λ^2 and R_λ. – – –, $\langle q^2\rangle$; - - - , $\langle\varepsilon\rangle$; —·—, R_λ; —··—, λ^2.

that R_λ is quite large ($\approx$850) at $t = 0$. Over the range $10 \leqslant t \leqslant 60$, its magnitude is small ($\approx$42 at $t = 10$, $\approx$ 38 at $t = 60$).

A requirement of equilibrium similarity is that $\langle q^2(t)\rangle$ must decay according to a power-law, namely

$$\frac{\langle q^2\rangle}{2} = A_q(-t_0)^m. \tag{3}$$

Since

$$\langle\varepsilon(t)\rangle = -\frac{1}{2}\frac{\mathrm{d}\langle q^2\rangle}{\mathrm{d}t} = -mA_q(t-t_0)^{m-1} \tag{4}$$

it follows that

$$\lambda^2(t) = -\frac{10}{m}\nu(t-t_0). \tag{5}$$

The magnitude of m can be inferred directly from $\mathrm{d}\lambda^2(t)/\mathrm{d}t$. A high-order polynomial fit was first applied to $\ln\lambda^2(t)$ vs $\ln t$. Only the fits are shown in figure 4 since they are virtually indistinguishable from the original data. For both the 240^3 and 270^3 simulations, the distributions of $\mathrm{d}\lambda^2/\mathrm{d}t$ become approximately constant in the range $25 \leqslant t \leqslant 60$. The horizontal lines in figure 4, when used in conjunction with (5), yield values of m equal to -1.097 and -1.12 for the 240^3 and 270^3 simulations respectively. The distribution of $\lambda^2/(-10\nu/m)$ is plotted in figure 5 for $m = -1.097$. Extrapolation of the linear fit over the range $20 \leqslant t \leqslant 60$ yields a value of 2 for t_0.

It follows from (3) and (4) that $\langle q^2(t)\rangle^{1/m}$ and $\langle\varepsilon(t)\rangle^{1/(m-1)}$ should vary linearly with time. This is indeed what is observed in figure 6 ($A \approx 0.25$); the two distributions follow each other closely since the magnitude of m is close to -1. It follows from (3) and (5) that

$$R_\lambda = \left(\frac{20\ A_q}{-3m\nu}\right)^{1/2}(t-t_0)^{(m+1)/2}. \tag{6}$$

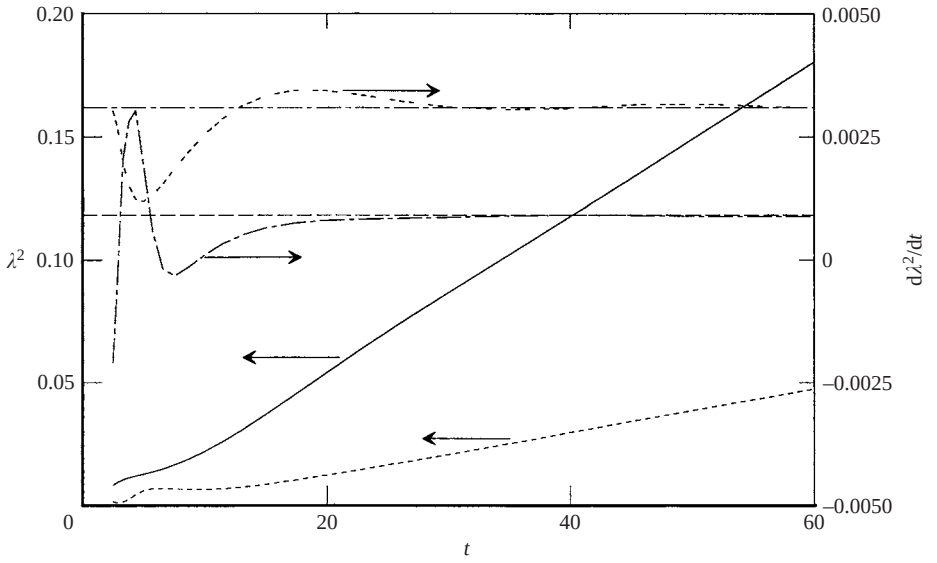

FIGURE 4. Dependence on t of $d\lambda^2/dt$. Fitted distributions to λ^2 are also shown. $d\lambda^2/dt$: --- ---, 240^3; —·—, 270^3. Fits to λ^2: —, 240^3; - - -, 270^3. Magnitudes of horizontal lines are used for estimating m via (5).

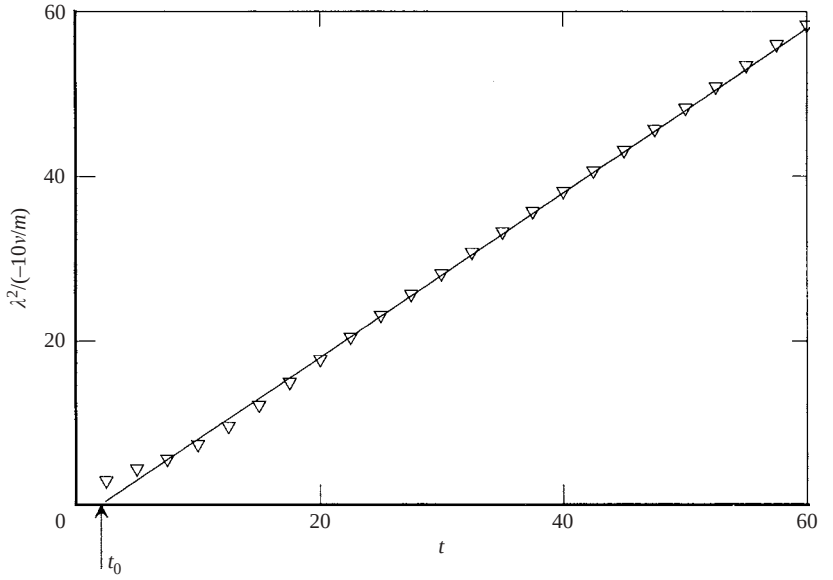

FIGURE 5. Temporal evolution of $\lambda^2/(-10\nu/m)$ for $m = -1.097$. Determination of virtual origin t_0. △, DNS data; —, linear fit over the range $t \geqslant 20$.

The data for R_λ compare favourably with (6) (figure 7) over the range where λ^2 grows linearly with t. Taken collectively, figures 2, 3 and 4 indicate that the behaviours of $\langle q^2(t)\rangle$, $\langle \varepsilon(t)\rangle$ and R_λ are fully consistent with equilibrium similarity.

The variations with respect to t of $\int_0^\infty E_\theta(k,t)\,dk$ and $\int_0^\infty k^2 E_\theta(k,t)\,dk$ (not shown here) indicated that, relative to $\int_0^\infty E(k,t)\,dk$ and $\int_0^\infty k^2 E(k,t)\,dk$, the onset of a

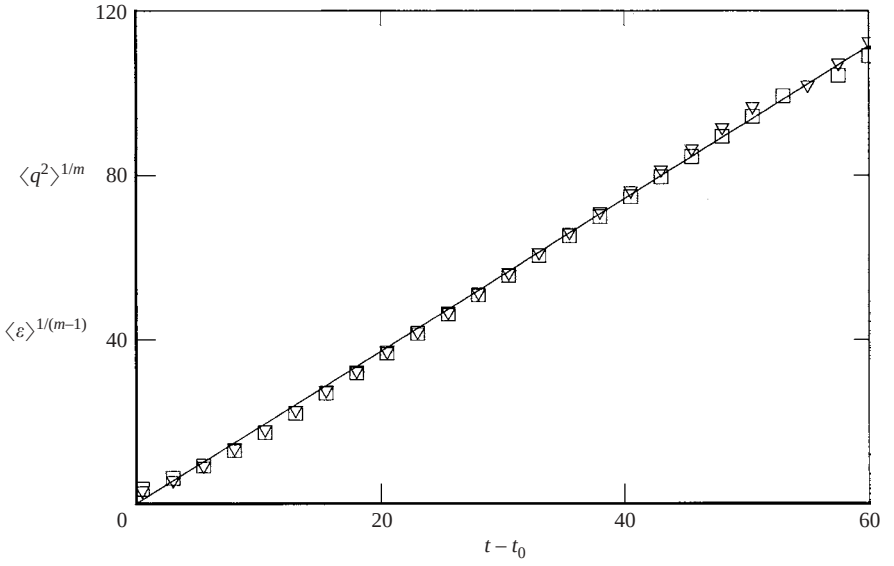

FIGURE 6. Evolution of $\langle q^2\rangle^{1/m}$ and $\langle \varepsilon\rangle^{1/(m-1)}$ as a function of $(t-t_0)$. △, $\langle q^2\rangle^{1/m}$; □, $\langle \varepsilon\rangle^{1/(m-1)}$; —, 1.86 $(t-t_0)$.

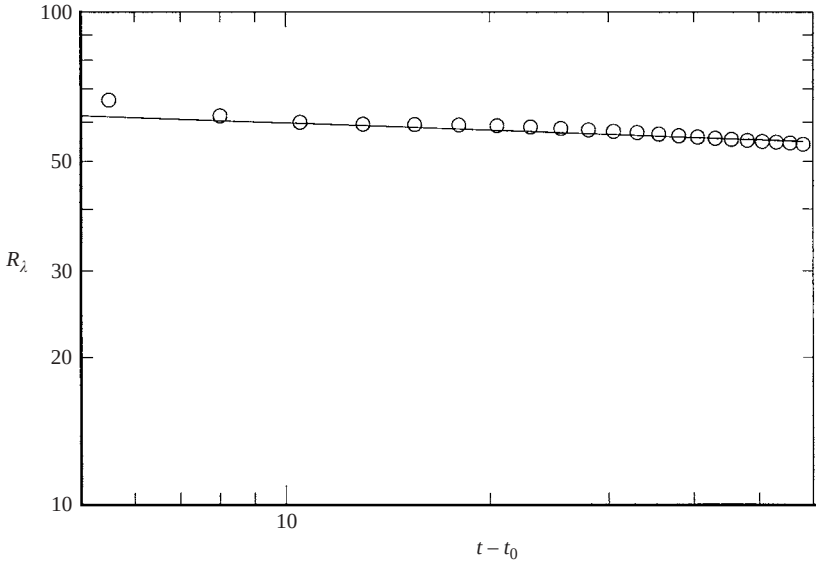

FIGURE 7. Variation of Taylor microscale Reynolds number R_λ with $(t-t_0)$. ○, DNS; ———, (6) with $A_q = 0.25$.

power-law behaviour for the scalar occurs at an increasingly larger value of t as Sc increases. In particular, the distributions for $Sc = 15$ suggested that a fully developed state of decay had not yet been reached at the largest time ($t = 60$). For the other values of Sc, the extent of the power-law range is narrower than for the velocity field. Over this range (typically $20 \lesssim t \lesssim 50$), the decay rate is steeper for the scalar than the velocity field. The magnitude of the exponent n was determined using a procedure similar to that used for estimating m, i.e. high-order polynomial fits were first applied

Sc	n	t_{θ_0}	Range of t
0.7	−1.44	−0.14	15–40
1	−1.41	0.08	15–40
3	−1.40	0.68	15–40
7	−1.39	2.36	25–50

TABLE 1. The magnitudes of n and t_{θ_0} in equation (7) for various Sc values.

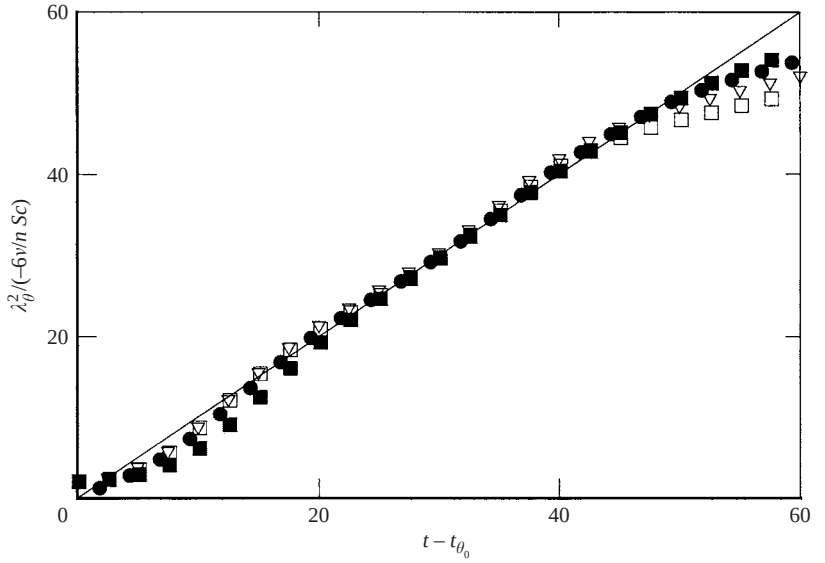

FIGURE 8. Variation of $\lambda_\theta^2/(-6\nu/n\,Sc)$ with $(t-t_{\theta_0})$. ○, $Sc=0.07$; □, 0.7; △, 1; ●, 3; ■, 7. ——, $\lambda_\theta^2/(-6\nu/n\,Sc)=(t-t_{\theta_0})$ with $n=-1.4$.

to $\ln\lambda_\theta^2$ vs $\ln t$ before differentiating λ_θ^2. The values of n were obtained by identifying the most likely plateaus in the distributions of $\mathrm{d}\lambda_\theta^2/\mathrm{d}t$, commensurate with the linear behaviour of λ_θ^2, namely

$$\lambda_\theta^2 = -\frac{6}{n}\frac{\nu}{Sc}(t-t_{\theta_0}), \tag{7}$$

where t_{θ_0} is the virtual origin for the scalar. The magnitudes of n and t_{θ_0} are shown in table 1. The table indicates that there is only a relatively small change in n between $Sc=0.7$ and $Sc=7$. There is, however, a systematic increase in t_{θ_0} as Sc increases. The magnitude of n is significantly larger than that of m, implying that the value of the scalar/velocity time scale ratio $R\equiv(\langle\theta^2\rangle/\langle\varepsilon\rangle)/(\langle q^2\rangle/\langle\varepsilon\rangle)$ is smaller than 1 (R is equal to m/n if $\langle\theta^2(t)\rangle$ and $\langle q^2(t)\rangle$ exhibit power-law behaviours). This is in contrast to values of R closer to 1 in earlier simulations (Orlandi & Antonia 2002) with different initial conditions (the scalar field at $Sc=0.7$ and $t=10$ was used as the starting point for simulations at different values of Sc). Note that a significant variation of R has also been noted in grid turbulence experiments, depending on the choice of initial conditions (see for example Zhou *et al.* 2000).

Distributions of $\lambda_\theta^2/(-6\nu/nSc)$ are plotted in figure 8 vs. $(t-t_{\theta_0})$. As expected, irrespective of Sc, the data follow the same linear distribution over the range of t

used to obtain n and t_{θ_0}. The departure from this distribution first occurs for $Sc = 0.7$ and at increasingly larger values of $(t - t_{\theta_0})$ as Sc increases.

4. Similarity of spectra and transfer functions

For the equilibrium similarity hypothesis, $E(k, t)$ and $T(k, t)$ are given by

$$E(k, t) = E_s(t)\tilde{E}(\tilde{k}) \tag{8}$$

and

$$T(k, t) = T_S(t)\tilde{T}(\tilde{k}), \tag{9}$$

where $E_s \equiv u^2\lambda$ and $T_s \equiv \nu u^2/\lambda$ are the similarity scales for E and T respectively and depend only on t, whereas $\tilde{E}$ and $\tilde{T}$ depend only on $\tilde{k} \equiv k\lambda$. Similarly, $E_\theta(k, t)$ and $T_\theta(k, t)$ are given by

$$E_\theta(k, t) = E_{\theta s}(t)\tilde{E}_\theta(\tilde{k}_\theta) \tag{10}$$

and

$$T_\theta(k, t) = T_{\theta s}(t)\ \tilde{T}_\theta(\tilde{k}_\theta), \tag{11}$$

where $E_{\theta s} \equiv \theta^2\lambda_\theta$ and $T_{\theta s} \equiv \nu_\theta\,\theta^2/\lambda_\theta$ are the similarity scales for E_θ and T_θ respectively and $\tilde{k}_\theta \equiv k\lambda_\theta$. The tilde denotes normalization according to G92.

We also consider two other types of normalization. The first uses Kolmogorov variables, i.e. $U_\kappa \equiv \nu^{1/4}\langle\varepsilon\rangle^{1/4}$ and η, so that $E(k, t) = U_\kappa^2\eta\, E^*(k^*)$ and $T(k, t) = U_\kappa^3 T^*(k^*)$ where $k^* \equiv k\eta$, the asterisk denoting normalization by U_κ and/or η. The second uses Batchelor variables $\theta_B \equiv (\langle\varepsilon_\theta\rangle/\gamma)^{1/2}$ and $\eta_B \equiv (\nu_\theta/\gamma)^{1/2} = \eta\, Sc^{-1/2}$ ($\gamma \equiv (\langle\varepsilon\rangle/\nu)^{1/2}$ is the mean strain rate), so that $E_\theta(k, t) = \theta_B^2\,\eta_B\, E^\dagger(k^\dagger)$ and $T_\theta(k, t) = \theta_B^2\,\gamma_{\eta_B}\, T^\dagger(k^\dagger)$, where $k^\dagger \equiv k\eta_B$.

Distributions of $\tilde{E}(\tilde{k})$ and $E^*(k^*)$ are shown in figures 9(a) and 9(b) respectively for six values of t, between $t = 10$ and 60. Although the collapse may be considered as reasonable for each type of normalization, the Kolmogorov scaled distributions for $k^* \gtrsim 0.2$ (figure 9b) tend to collapse better than those of $\tilde{E}(\tilde{k})$ for $\tilde{k} \gtrsim 10$ (figure 9a). (The improved collapse will be more easily discerned in § 6 in linear plots of $\tilde{k}^4\tilde{E}(\tilde{k})$ and $k^{*\,4}E^*(k^*)$). The same amount of scatter appears at small $\tilde{k}$ or k^* in the two types of normalization and remains unchanged when the data are replotted (not shown here) in the form of $\tilde{k}\tilde{E}(\tilde{k})$ vs. $\ln\tilde{k}$ or $k^*E^*(k^*)$ vs. $\ln k^*$. Scaling on Kolmogorov variables is not expected to apply at small wavenumbers and the present spectra conform with this expectation. That the collapse based on Kolmogorov variables appears to extend over a substantial range of $k*$ is probably due to the present small values of R_λ.

Distributions of the products $\tilde{k}\,\tilde{T}\,(\tilde{k})$ and $k^*\,T^*\,(k^*)$ are plotted against $\ln\tilde{k}$ and $\ln k*$ in figures 10(a) and 10(b) respectively. For wavenumbers beyond the peaks in these distributions, there is better collapse for $k^*\,T^*\,(k^*)$ (figure 10b) than $\tilde{k}\,\tilde{T}\,(\tilde{k})$ (figure 10a). In the latter case, there is a systematic decrease in the magnitude as t increases (as indicated by the arrow in figure 10a). For wavenumbers on the left of the peak, the collapse in figure 10(b) appears to be of comparable quality to that in figure 10(a). Oscillations on the left of the peak can be observed in figures 10(a) and 10(b). Similar wiggles are also noticeable in the energy spectra and are caused primarily by the small statistical samples in low-k shells (A. Wray, private communication).

In figure 11(a), the collapse of the distributions of $\tilde{E}_\theta(\tilde{k}_\theta)$ for $Sc = 0.7$ is imperfect at both small and large wavenumbers. There is a crossover near $\tilde{k}_\theta \approx 3$; at smaller $\tilde{k}_\theta$, the magnitude tends to increase with time whereas the inverse occurs at larger

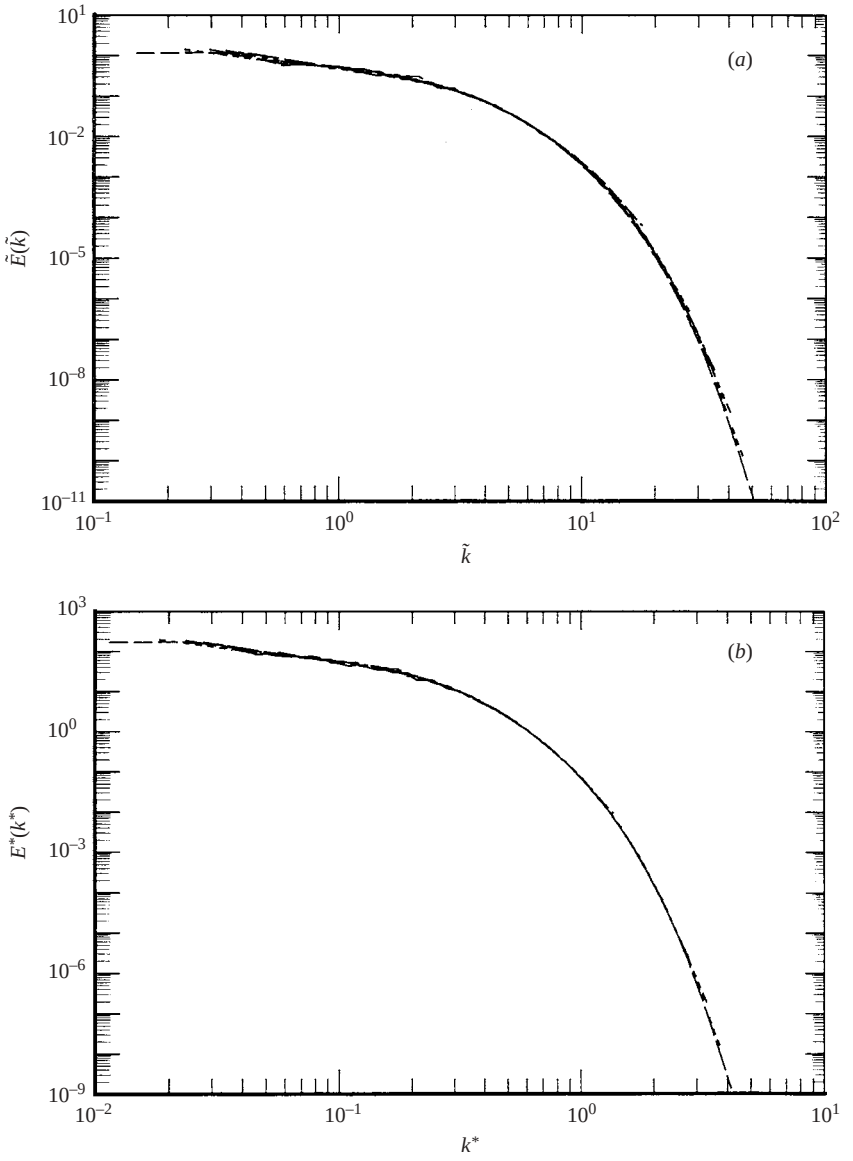

FIGURE 9. Three-dimensional energy spectra normalized using (*a*) G92 and (*b*) Kolmogorov variables. – ––, $t = 10$; - - -, 20; —·—, 30; — · ·—, 40; - - - - - -, 50; — —, 60.

$\tilde{k}_\theta$. This effect, illustrated by the two arrows, is also observed at larger values of *Sc*. By contrast, distributions of $E_\theta^\dagger(k^\dagger)$ (figure 11*b*) collapse approximately for $k^\dagger \gtrsim 0.3$. This is also independent of *Sc*, although the collapse occurs at larger times as *Sc* increases. For $k^\dagger \lesssim 0.3$ the effect of increasing t on $E_\theta^\dagger(k^\dagger)$ is comparable to that observed in $\tilde{E}_\theta(\tilde{k}_\theta)$. On the basis of figure 11 and virtually identical results at larger values of *Sc*, we can claim that Batchelor normalization collapses the scalar spectra adequately for wavenumbers approaching and exceeding $k^\dagger = 1$. Such a collapse is not seen when G92 variables are used. These observations apply to the distributions of

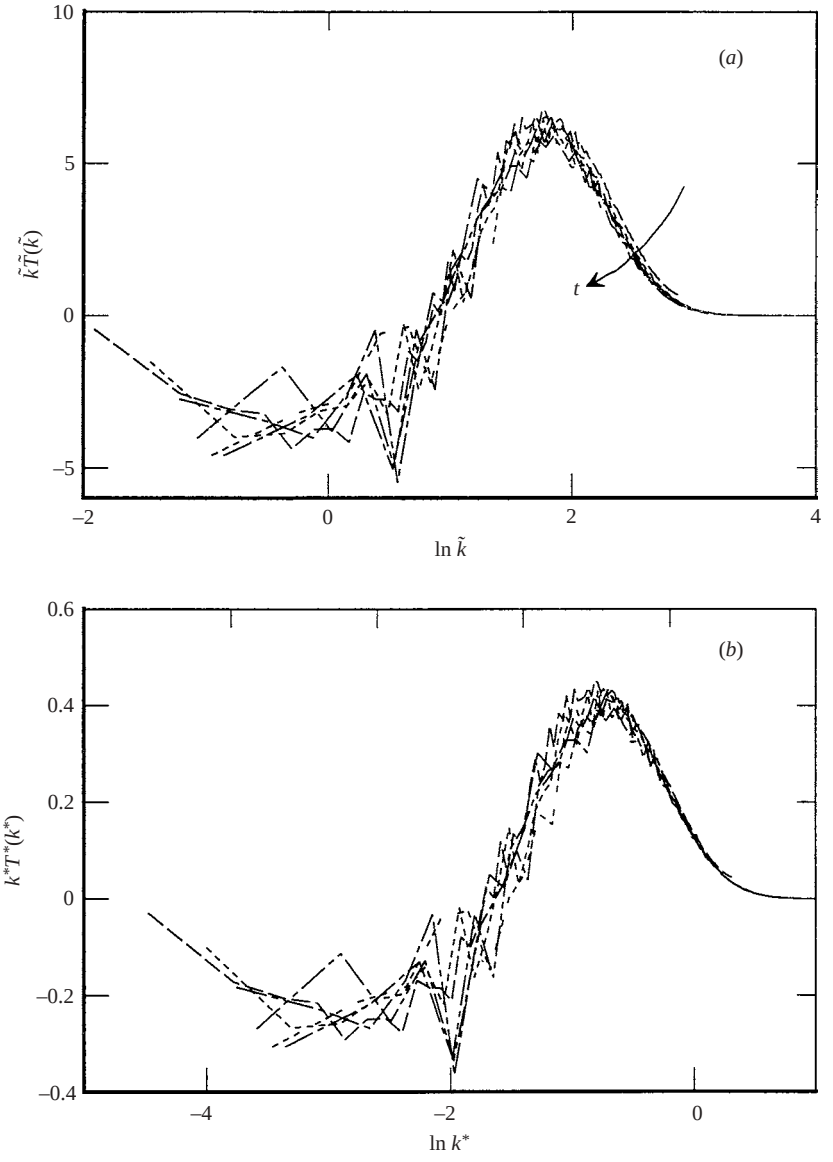

FIGURE 10. Product of the wavenumber and energy transfer function, normalized using (*a*) G92 and (*b*) Kolmogorov variables. – – –, $t = 10$; - - -, 20; — - —, 30; — - - —, 40; - - - - - -, 50; ——, 60.

$\tilde{k}_\theta \tilde{T}_\theta(\tilde{k}_\theta)$ (figure 12*a*) and $k^\dagger T^\dagger(k^\dagger)$ (figure 12*b*); only results for $Sc = 3$ are shown here (figure 12) since distributions at other values of Sc are similar to those in figure 12.

The effect of Sc on the scalar spectra and transfer functions is more readily appreciated from distributions of these quantities at a fixed (and sufficiently large) t but for different values of Sc, plotted on the same figure. Figure 13 indicates that, regardless of whether G92 (figure 13*a*) or Batchelor variables (figure 13*b*) are used, there is no discernible effect of Sc on the spectra provided the wavenumber is sufficiently large ($\tilde{k}_\theta \gtrsim 3$ in figure 13(*a*) or $k^\dagger \gtrsim 0.3$ in figure 13(*b*)). The results for the transfer functions (figure 14) exhibit some differences relative to those in

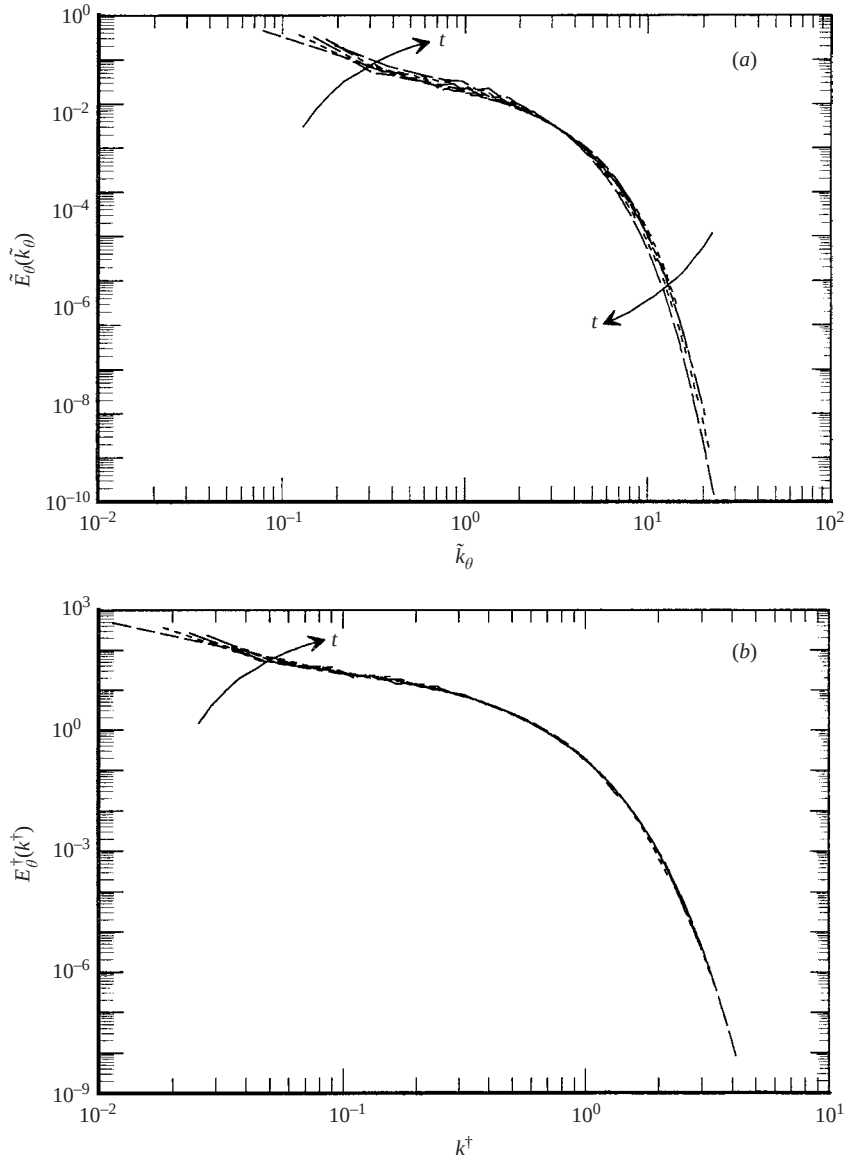

FIGURE 11. Three-dimensional scalar spectra for $Sc = 0.7$, normalized using (*a*) G92 and (*b*) Batchelor variables. – – –, $t = 10$; - - -, 20; — - —, 30; — - - —, 40; - - - - - -, 50; — —, 60.

figure 12. For wavenumbers below either $\tilde{k}_\theta \approx 4$ (figure 14*a*) or $k^\dagger \approx 0.6$ (figure 14*b*), it is difficult to detect an effect of Sc on $\tilde{k}_\theta\, \tilde{T}_\theta\, (\tilde{k}_\theta)$ or $k^\dagger\, T_\theta^\dagger\, (k^\dagger)$, because of the scatter. For larger wavenumbers, there seems to be a systematic decrease in the magnitude of those products as Sc increases. The effect, however, is more pronounced for $\tilde{k}_\theta\, \tilde{T}_\theta\, (\tilde{k}_\theta)$ (figure 14*a*) than $k^\dagger\, T_\theta^\dagger(k^\dagger)$ (figure 14*b*).

5. Calculation of energy and scalar transfer functions

The transfer functions $T(k, t)$ and $T_\theta(k, t)$ are related to $E(k, t)$ and $E_\theta(k, t)$ via (1) and (2). The dependence of $\tilde{T}(k)$ or $\tilde{E}(k)$ can be readily obtained after substituting

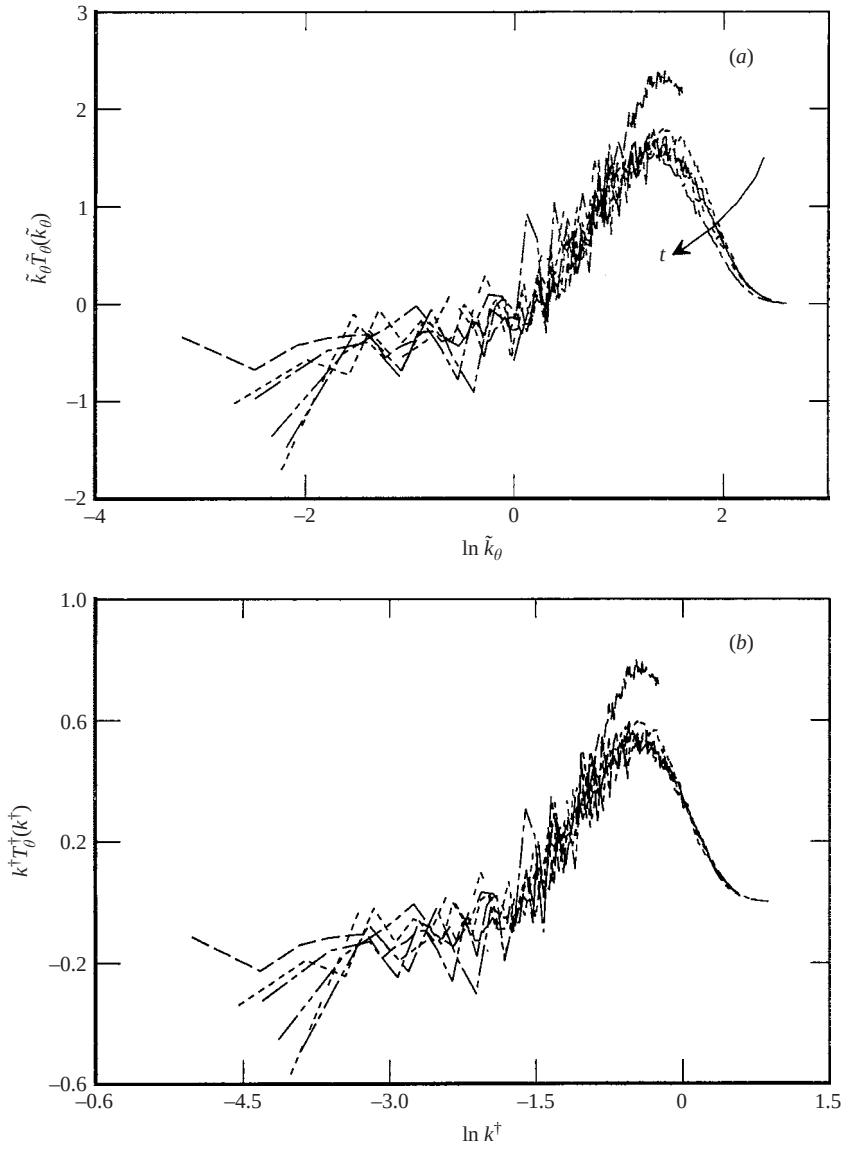

FIGURE 12. Wavenumber–scalar transfer function product for $Sc = 3$, normalized using (*a*) G92 and (*b*) Batchelor variables. – – –, $t = 10$; - - -, 20; — - —, 30; — - - —, 40; - - - - - -, 50; — —, 60.

(8) and (9) into (1) and making use of relations (3), (4) and (5). This relation was written in G92 and is rewritten below (because of the different notation used here):

$$\tilde{T}(\tilde{k}) = 2\tilde{k}^2\, \tilde{E}(\tilde{k}) - 5(m^{-1} + 2)\, \tilde{E}(\tilde{k}) - m^{-1} \tilde{E}'(\tilde{k}) \tag{12}$$

where the prime denotes differentiation with respect to $\tilde{k}$. As noted in G92, $\tilde{T}(\tilde{k})$ depends on the initial conditions via $\tilde{E}(\tilde{k})$ and the exponent m.

Substituting (10) and (11) into (2) and making use of the following power-law relations:

$$\langle \theta^2(t) \rangle = A_\theta (t - t_{\theta_0})^n, \tag{13}$$

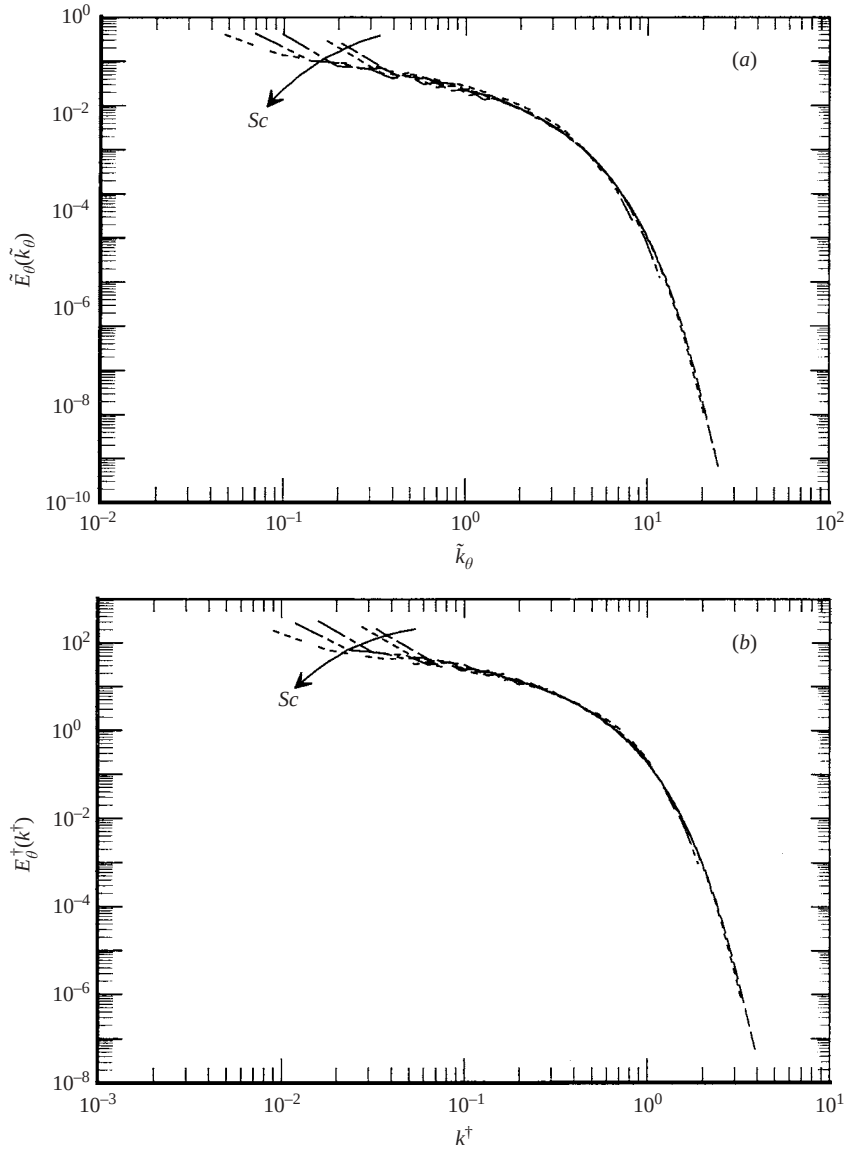

FIGURE 13. Dependence on Sc of the three-dimensional scalar spectrum, normalized using (*a*) G92 and (*b*) Batchelor variables. – – –, $Sc = 0.7$ ($t = 40$); - - -, 1(40); — - —, 3(40); — - - —, 7(50); - - - - - -, 15(60).

$$\langle \varepsilon_\theta(t) \rangle = -\frac{1}{2}\frac{\mathrm{d}\langle\theta^2\rangle}{\mathrm{d}t} = \frac{-n}{2} A_\theta (t - t_{\theta_0})^{n-1}, \tag{14}$$

together with (7), it is relatively straightforward to obtain an expression for $\tilde{T}_\theta(\tilde{k}_\theta)$ in terms of $\tilde{E}_\theta(\tilde{k}_\theta)$. The final expression may be written

$$\tilde{T}_\theta(\tilde{k}_\theta) = 2\tilde{k}_\theta^2\, \tilde{E}_\theta(\tilde{k}_\theta) - 3(n^{-1}+1)\, \tilde{E}_\theta(\tilde{k}_\theta) - 3n^{-1}\, \tilde{k}_\theta\, \tilde{E}'_\theta(\tilde{k}_\theta), \tag{15}$$

where the prime denotes differentiation with respect to $\tilde{k}_\theta$. This result differs slightly from that given by George (1992*b*) because a different definition of λ_θ was used in

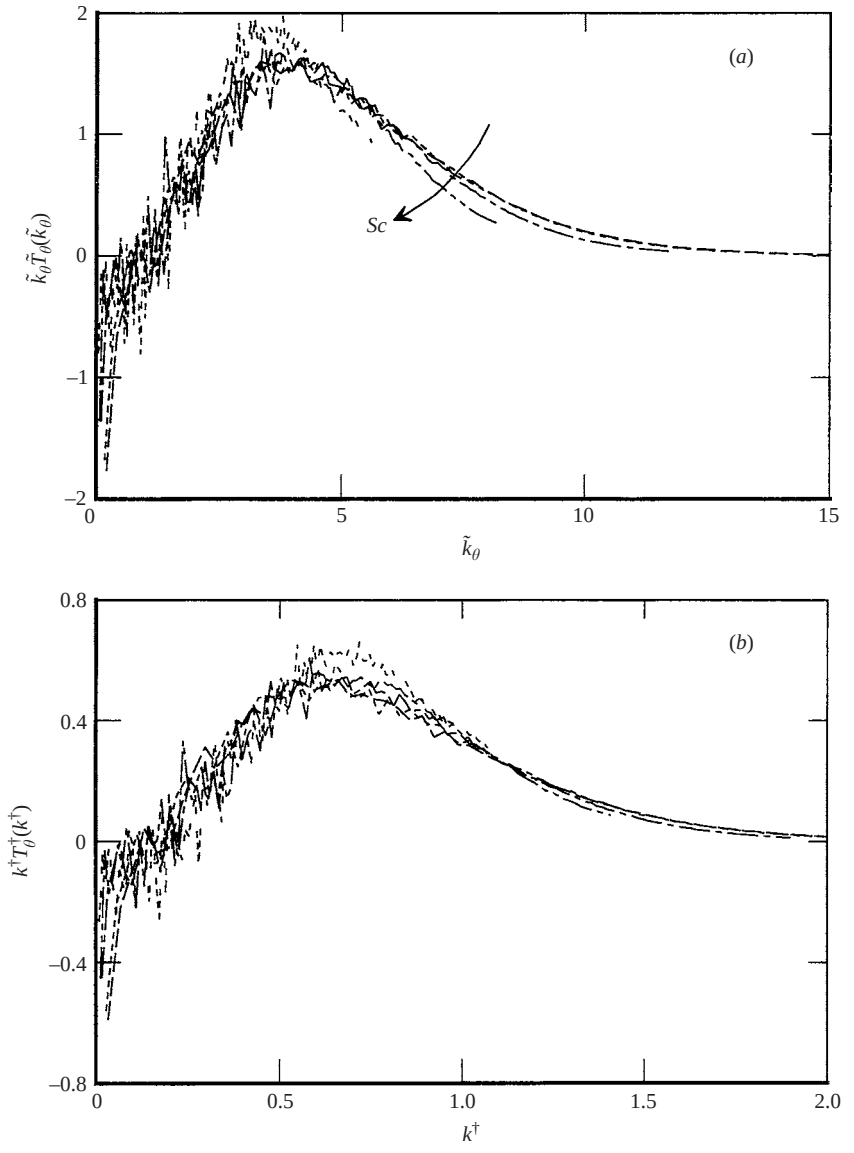

FIGURE 14. Dependence on Sc of the wavenumber–scalar transfer function product, normalized using (a) G92 and (b) Batchelor variables. – – –, $Sc = 0.7$ ($t = 40$); - - -, 1(40); — - —, 3(40); — - - —, 7(50); - - - - - -, 15(60).

that paper. The dependence of $\tilde{T}_\theta(\tilde{k}_\theta)$ on initial conditions reflects that of $\tilde{E}_\theta(\tilde{k}_\theta)$ and the exponent n.

Note that as Sc does not appear explicitly in (15), any dependence of $\tilde{T}_\theta(\tilde{k}_\theta)$ on Sc should only reflect a possible dependence on Sc of $\tilde{E}_\theta(\tilde{k}_\theta)$ and n. A comparison between directly computed distributions of $\tilde{T}(\tilde{k})$ and $\tilde{T}_\theta(\tilde{k}_\theta)$ and those calculated using (12) and (15) is given in figures 15(a) and 16(a) respectively. In each case, the agreement is good over nearly the complete wavenumber range. In particular, the agreement for $\tilde{T}(\tilde{k})$ (figure 15a) is of comparable quality to that reported by George & Wang (2002) for the DNS data of Wray. In figures 15 and 16, the distributions are

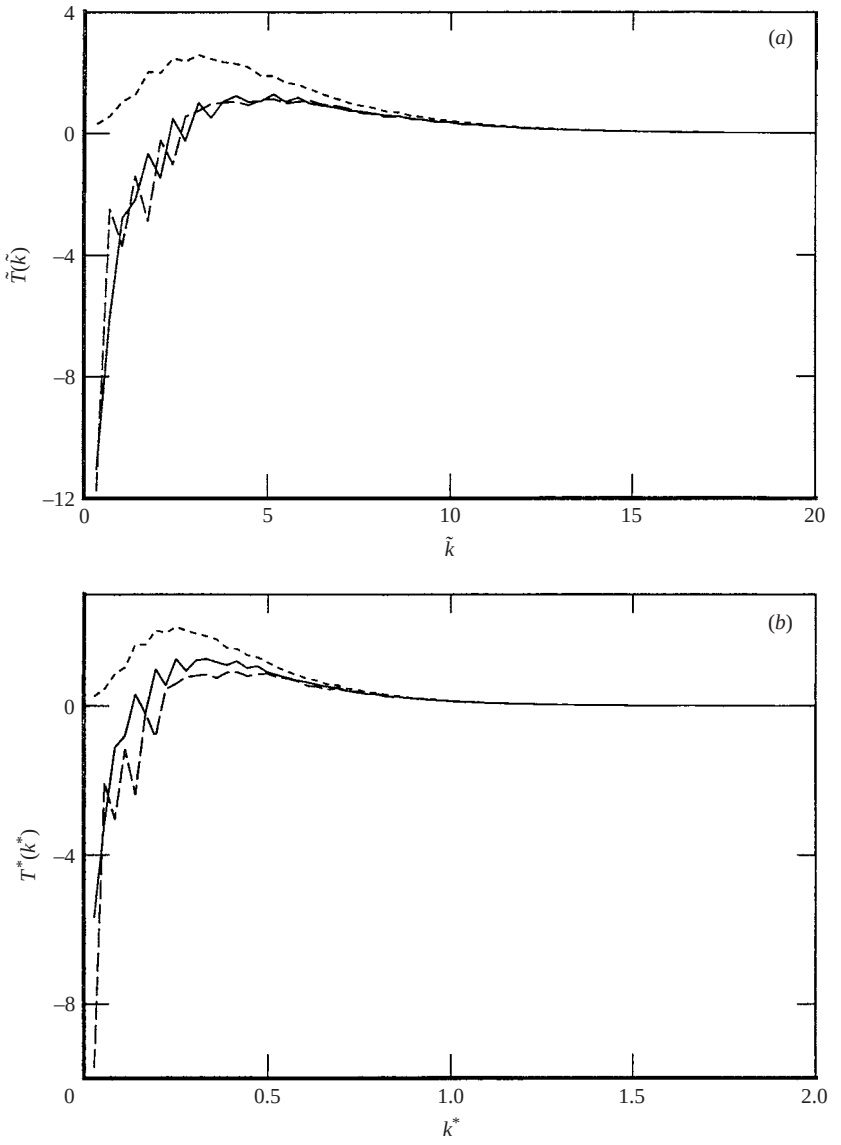

FIGURE 15. Comparison between DNS and calculated distributions of the energy transfer function, normalized using (*a*) G92 and (*b*) Kolmogorov variables. – – –, DNS; —, calculation based on (12), in (*a*), and (A 1) in (*b*); - - -, calculation based on the approximation $T(k,t) \approx 2\nu k^2 E(k,t)$.

at $t = 40$ but comparable agreement between the data and the calculations was also found at $t = 50$ and 60. Only distributions for $Sc = 1$ are shown in figure 16 since a similar level of agreement was found for other values of Sc.

Calculated distributions of $T^*(k^*)$ and $T_\theta^\dagger(k^\dagger)$ were also determined by assuming a possible similarity using either Kolmogorov or Batchelor variables. Resulting expressions for these calculations are given in the Appendix. Figure 15(*b*) indicates that the calculation overestimates the DNS $T^*(k^*)$ data for $k^* \lesssim 0.5$. On the other hand, the calculated distribution of $T_\theta^\dagger(k^\dagger)$ lies below the DNS data for $k^\dagger \lesssim 0.7$

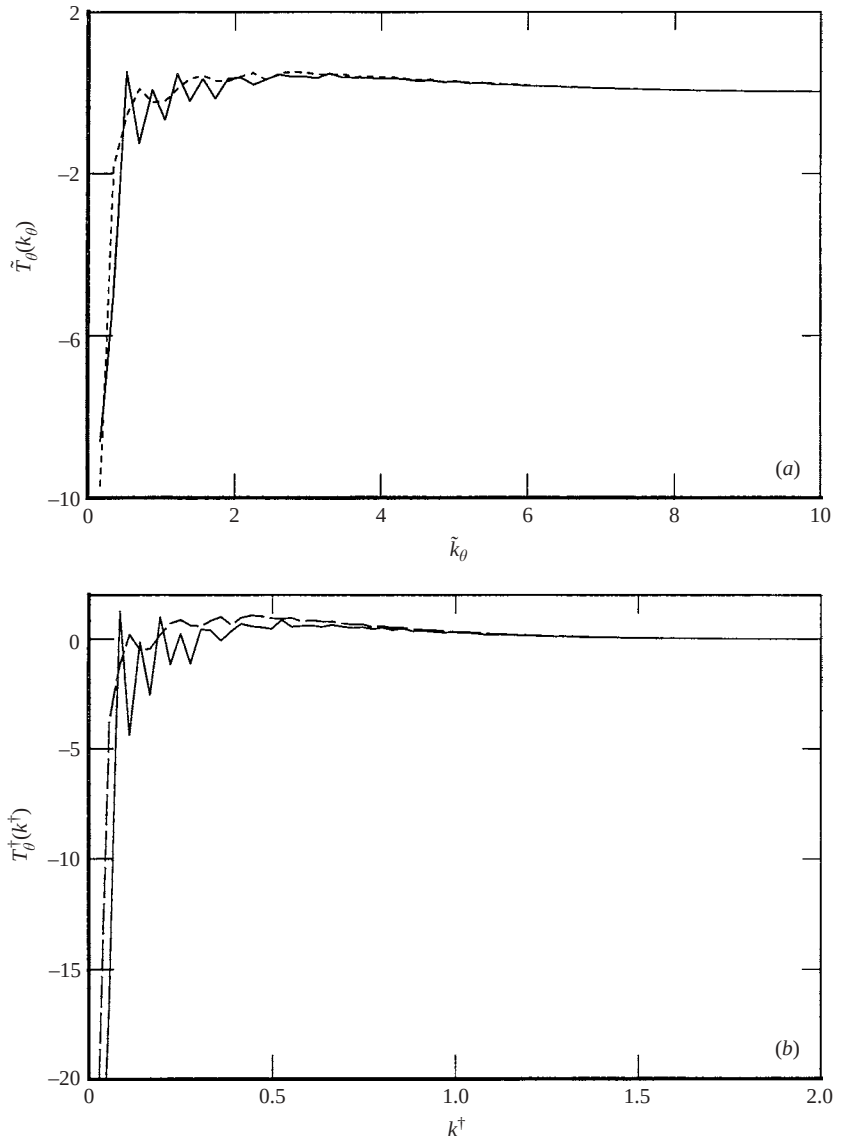

FIGURE 16. Comparison between DNS and calculated distributions of the scalar transfer function, normalised using (*a*) G92 and (*b*) Batchelor variables. $Sc = 1$. – – –, DNS; —, calculation. In (*a*), the calculation is based on (15); in (*b*), it is based on (A 2).

(figure 16*b*). The discrepancy between calculated and DNS data in figures 15(*b*) and 16(*b*) is not surprising since the Kolmogorov and Batchelor normalizations are expected to be relevant only for sufficiently small scales. It is appropriate to underline that, although Kolmogorov and Batchelor normalized distributions of $E(k, t)$ and $E_\theta(k, t)$, e.g. figures 9–11, indicate a better collapse than for G92, there is no rigorous basis for either Kolmogorov or Batchelor similarity at all scales.

George & Wang (2002) noted that the universal equilibrium range idea of Kolmogorov (1941) whereby $\partial E/\partial t$ can be neglected when k is sufficiently large, did not apply even at the highest Reynolds numbers available. We similarly note here

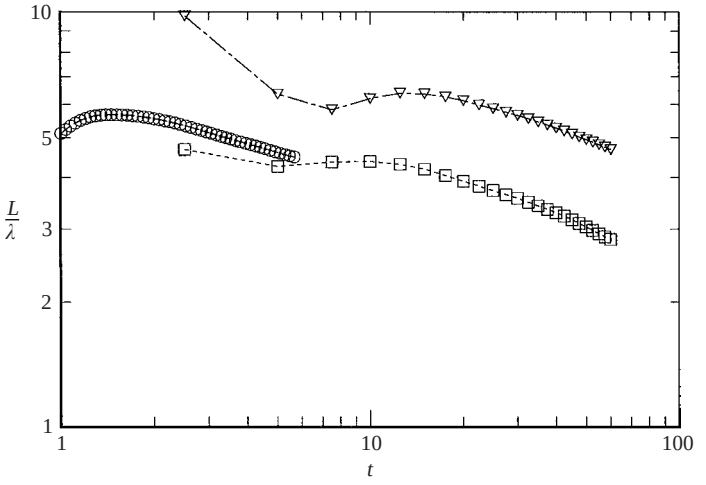

FIGURE 17. Ratio of integral length scale and Taylor microscale. Comparison with Wray (1998). ○, Wray (1998); □, present (240^3); △, present (270^3).

that the calculation of the transfer term based on the approximation

$$T(k,t) \approx 2\nu k^2 E(k,t)$$

is inadequate except at large wavenumbers (figures 15*a* and 15*b*). For the present small Reynolds numbers, the neglect of $\partial E/\partial t$ is only justifiable at the smallest dissipative scales ($\tilde{k} \gtrsim 15$ in figure 15(*a*) or $k^* \gtrsim 1$ in figure 15(*b*)). This seems to be in contrast to the present observation, as well as that inferred from previous HIT simulations (e.g. Mansour & Wray 1994) – also for small Reynolds numbers – that the distributions of $E(k,t)$ and $T(k,t)$ collapse adequately, at sufficiently large k, when scaled on Kolmogorov variables.

6. Further assessment of consequences of G92

Ideally, the DNS database should be adequately resolved both at the lowest and largest wavenumbers in order to be able to test any similarity proposal adequately. In the context of HIT, Wang & George (2002) indicated that the absence of scales an order of magnitude below the peak in the energy spectrum can affect the determination of the energy and more especially the integral length scale L. The shift of the energy peak towards lower wavenumbers as the flow decays exacerbates this difficulty. These authors also indicated that all values of L obtained from both numerical and experimental data (in the latter case, L is usually the three-dimensional integral length scale) are questionable. In particular, the ratio L/λ is not constant, as required by G92, but decreases during decay. The present values of L/λ (figure 17) are consistent with this trend as are the data of Wray and those we have obtained, also using a finite-difference method, for a 270^3 grid. Wang & George (2002) used a spectral model to correct the results of Wray (1998). After correction, L/λ (figure 8(*a*) of their paper) decayed much more slowly over the similarity range than the uncorrected ratio. The integral length scales L and L_θ are defined by

$$L = \frac{\pi}{2\langle q^2\rangle}\int_0^\infty \frac{E(k)}{k}\,\mathrm{d}k, \quad L_\theta = \frac{\pi}{2\langle \theta^2\rangle}\int_0^\infty \frac{E_\theta(k)}{k}\,\mathrm{d}k.$$

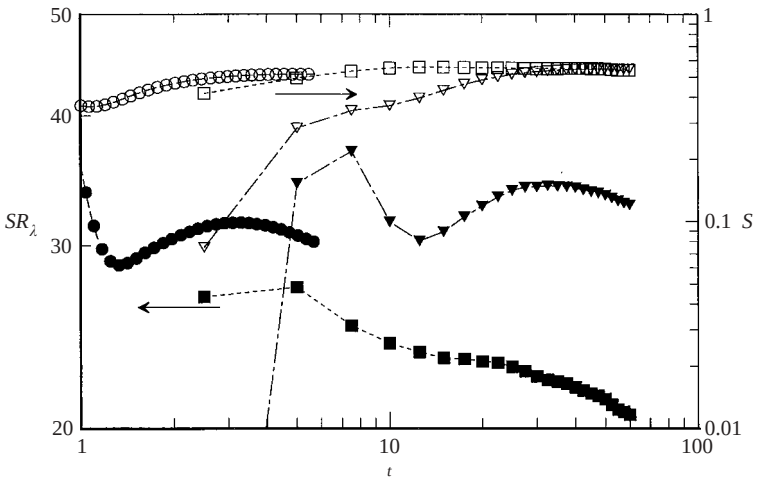

FIGURE 18. Velocity derivative skewness S and product SR_λ. Comparison with Wray (1998). ○, Wray (1998); □, present (240^3); ▽, present (270^3). Open and filled in symbols are for S and SR_λ respectively.

For the present simulations, the integrands have not yet started to return to zero at the smallest k, thus indicating that the largest scales are not adequately resolved. This lack of resolution is accentuated when t increases and is reflected in the distributions of L/λ and also L_θ/λ_θ (not shown here).

The present 270^3 DNS data has at $t = 60$ approximately the same value of $R_\lambda (\approx 60)$ as that of Wray ($R_\lambda \approx 58.4$ at $t = 5.72$). Despite this, the present value of $m (\approx -1.12)$ as inferred in figure 4 is, over the range $20 \leqslant t \leqslant 60$, comparable to that ($\approx -1.13$) we estimate from Wray's (1998) data. Wang & George (2002) used results from a slightly different simulation by Wray which was meant to mimic the Comte-Bellot & Corrsin (1971) experiment, starting from the same initial spectrum as for the AGARD run but using a different time advance and different dealiasing. They obtained a value of -1.5 for m, in the range $5 \lesssim t \lesssim 6$.

Figure 18 shows that the magnitude of $S \equiv \langle (\partial u/\partial x)^3 \rangle / \langle (\partial u/\partial x)^2 \rangle^{3/2}$, the skewness of the velocity derivative, attained a constant value (≈ 0.55) for $t \gtrsim 20$. This trend, also evident in Wray's data as well as the present 270^3 data, implies that the product SR_λ, also shown in figure 18, must decrease with t over at least part of the power-law region. Note that the time evolutions for Wray and the present 270^3 simulation are similar, both exhibiting local minima and maxima before decaying at the largest values of t.

The non-constancy of SR_λ is of concern since it violates an important consequence of G92. It is therefore important to assess the accuracy with which this product and, in particular S, has been estimated. In figure 18, S was estimated via the relation (e.g. Kerr 1985; G92)

$$S(t) = -\frac{3(30)^{1/2}}{14} \frac{\int_0^\infty k^2 T(k,t)\,\mathrm{d}k}{\left[\int_0^\infty k^2 E(k,t)\,\mathrm{d}k\right]^{3/2}}. \tag{16}$$

After multiplying (1) with k^2 and integrating with respect to k, S can be written (as in G92) as

$$S(t) = S_1(t) + S_2(t),$$

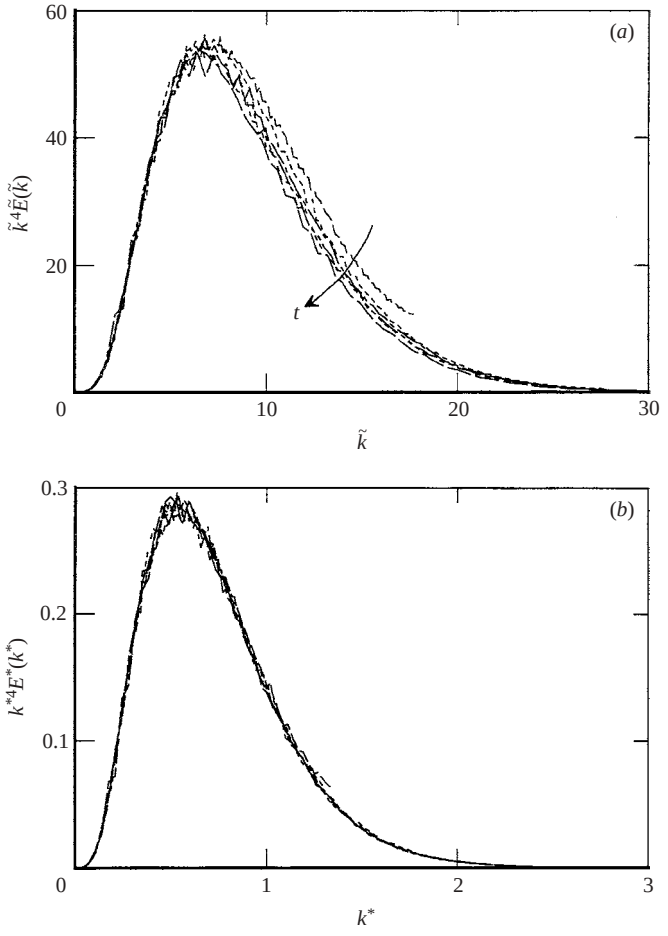

FIGURE 19. Distributions of (*a*) $\tilde{k}^4\tilde{E}(\tilde{k})$ and (*b*) $k^{*4}E^*(k^*)$ for the present (240^3) simulation. The arrow in (*a*) is in the direction of increasing t.

where

$$S_1(t) = -\frac{30^{1/2}}{14}\frac{\partial/\partial t\int_0^\infty k^2E(k,t)\,\mathrm{d}k}{\left[\int_0^\infty k^2E(k,t)\,\mathrm{d}k\right]^{3/2}} \tag{17}$$

and

$$S_2(t) = -\frac{3(30)^{1/2}}{14}\frac{\nu\int_0^\infty k^4E(k,t)\,\mathrm{d}k}{\left[\int_0^\infty k^2E(k,t)\,\mathrm{d}k\right]^{3/2}}. \tag{18}$$

Expression (17) can be simplified to

$$S_1(t) = \frac{30}{7R_\lambda}\frac{m-1}{m}. \tag{19}$$

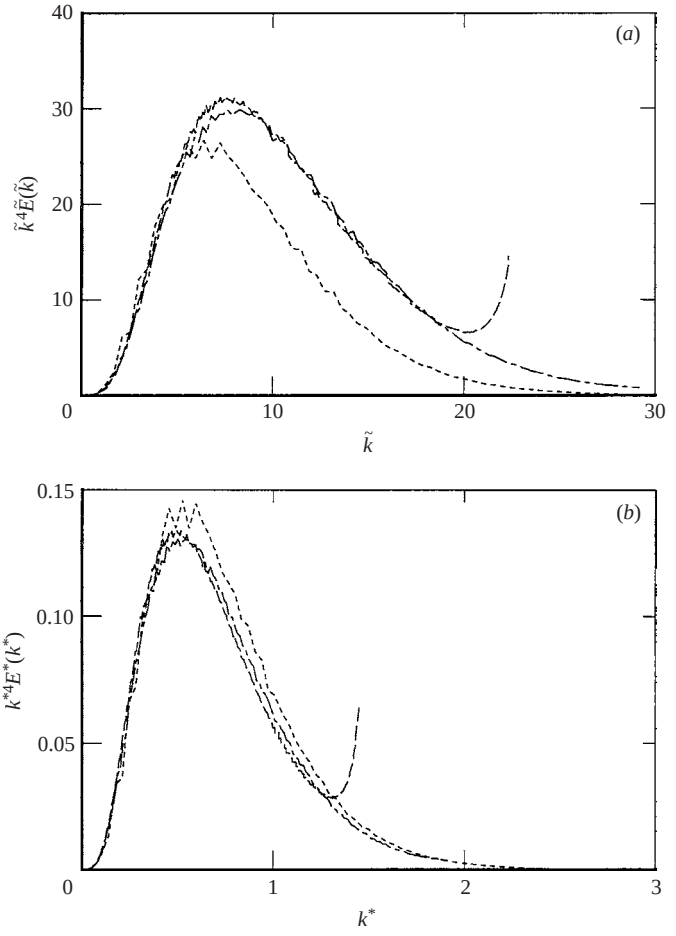

FIGURE 20. Distributions of (*a*) $\tilde{k}^4\tilde{E}(\tilde{k})$ and (*b*) $k^{*4}E^*(k^*)$. Comparison with Wray (1998). Wray (1998) – – –, $t=3.6$ ($R_\lambda \approx 61.5$; present (240^3) - - -, $t=60$ ($R_\lambda = 38.3$); present (270^3) — · — $t=60 (R_\lambda \approx 62)$.

The magnitude of $S_2(t)$ should be unaffected regardless of the scaling that is used. With G92, (18) can be written as

$$S_2(t) = -\frac{3(30)^{1/2}}{14R_\lambda} \frac{\int_0^\infty \tilde{k}^4 \tilde{E}(\tilde{k})\,\mathrm{d}\tilde{k}}{\left[\int_0^\infty \tilde{k}^2 \tilde{E}(\tilde{k})\,\mathrm{d}\tilde{k}\right]^{3/2}}. \tag{20}$$

Using the Kolmogorov normalization, (18) is given by

$$S_2(t) = -\frac{3(30)^{1/2}}{14} \frac{\int_0^\infty k^{*4} E^*(k^*)\,\mathrm{d}k^*}{\left[\int_0^\infty k^{*2} E^*(k^*)\,\mathrm{d}k^*\right]^{3/2}}. \tag{21}$$

Although $S_1(t)$ is of opposite sign to $S_2(t)$, its magnitude is quite small compared to that of $S_2(t)$. For the present 240^3 simulation, $S_1(t)$ increases from 0.009 at $t=20$

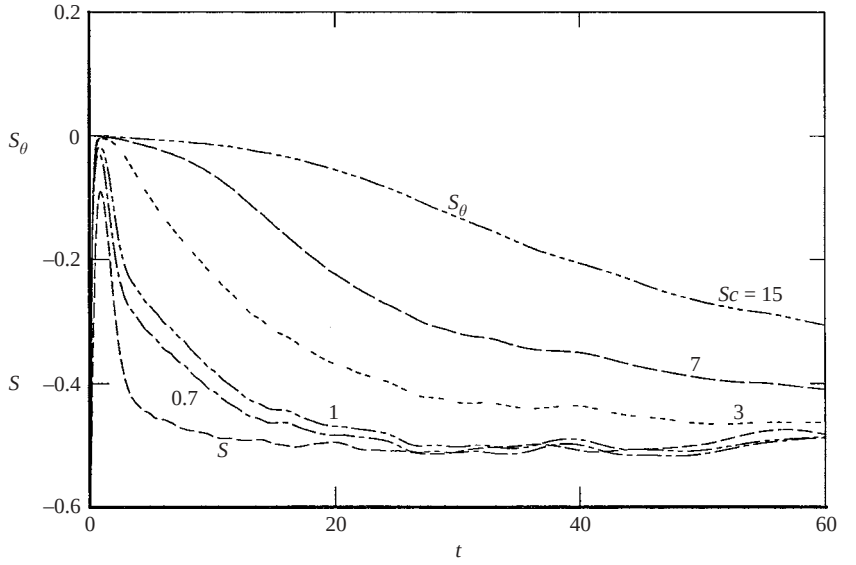

FIGURE 21. Temporal evolution of mixed velocity–scalar derivative skewness $S_\theta(t)$ for various values of Sc. The distribution of $S(t)$ is included for comparison. – – –, $Sc = 0.7$; - - -, 1; — - —, 3; — - - —, 7; - - - - - -, 15.

to 0.01 at $t = 60$. Given that R_λ varies with t, comparing (20) with (21) suggests that the validity of G92 precludes Kolmogorov similarity for the small-scales and vice versa. The appearance of k^4 in the numerator of (18) does, however, mean that it is important to ensure adequate closure of this integrand before any conclusion concerning the behaviour of $S(t)$ can be reached.

In figure 19, we plot $\tilde{k}^4\tilde{E}(\tilde{k})$ and $k^{*4}E^*(k^*)$ for the present 240^3 simulation and values of t in the range 10 to 60. Whilst the distributions at $t = 10$ do not close, all other distributions return to zero satisfactorily. Figure 1 indicates that the small-scale resolution improves as t increases, the largest value of k^* increasing from about 2.2 at $t = 20$ to about 4.2 at $t = 60$. The distributions of $\tilde{k}^4\tilde{E}(\tilde{k})$ (figure 19*a*) evolve with time in the direction of the arrow so that the integral decreases with t, allowing for the partial compensatory effect associated with the integral in the denominator of (20). This decrease is insufficient to offset the decrease in R_λ so that $S_2(t)$ becomes constant at sufficiently large t. The excellent collapse in figure 19(*b*) confirms our earlier conclusion, based on figures 11(*b*) and 12(*b*), that Kolmogorov normalization describes the small-scale motion more accurately than G92. The conclusion regarding the constancy of $S(t)$ at sufficiently large t would be more difficult to sustain as the Reynolds number of the simulation, and therefore the local value of R_λ, is increased. For example, figure 20 indicates that even a mild increase in R_λ impairs our ability to close the distribution of $k^4E(k, t)$. For the 270^3 simulation, the distribution at $t = 60$ has not quite returned to zero at $k^* \approx 2$. Wray's (1998) distribution at $t = 3.6$ is inadequately resolved, the energy pile-up at the largest $\tilde{k}$ or k^* reflecting the dealiasing due to the spectral cutoff in the pseudospectral method. Comparison between figures 20(*a*) and 20(*b*) highlights the greater sensitivity on R_λ of $E(\tilde{k})$, relative to $E^*(k^*)$.

The mixed velocity–scalar derivative skewness

$$S_\theta = \langle(\partial u/\partial x)(\partial\theta/\partial x)^2\rangle / \left(\langle(\partial u/\partial x)^2\rangle^{1/2}\langle(\partial\theta/\partial x)^2\rangle\right)$$

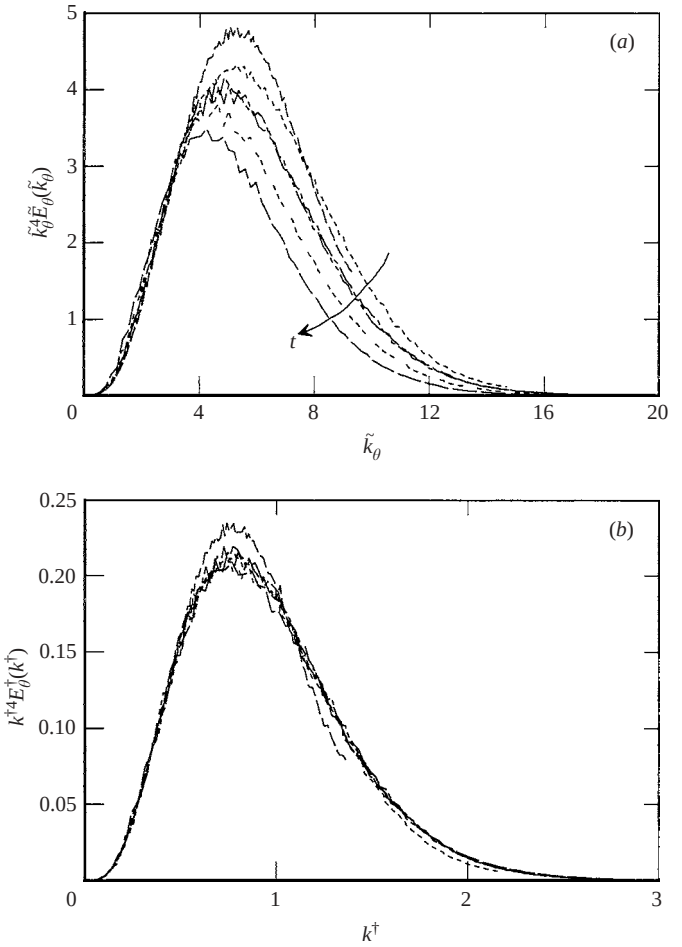

FIGURE 22. Distributions of $k^4 E_\theta(k)$ at $Sc = 1$ normalized using (*a*) G92 and (*b*) Batchelor variables. (*a*) $\tilde{k}_\theta^4 \tilde{E}_\theta(\tilde{k})$, (*b*) $k^{\dagger 4} E_\theta^\dagger(k^\dagger)$. – – –, $t = 10$; - - -, 20; — · —, 30; — · · —, 40; - - · - - -, 50; — —, 60.

can be deduced from the spectral expression

$$S_\theta(t) = -\frac{2}{15^{1/2}} \frac{\displaystyle\int_0^\infty k^2 T_\theta(k,t)\,\mathrm{d}k}{\left[\displaystyle\int_0^\infty k^2 E(k,t)\,\mathrm{d}k\right]^{1/2} \left[\displaystyle\int_0^\infty k^2 E_\theta(k,t)\,\mathrm{d}k\right]}.$$

The resulting distributions of $S_\theta(t)$ (figure 21) indicate an approach toward a constant, at least when Sc is not significantly larger than 1. For $Sc = 0.7$ and 1, constancy is achieved for $t \gtrsim 20$, the magnitude of the constant being approximately equal to that of $S(t)$ (the latter distribution is included in the figure). For $Sc = 3$, $S_\theta(t)$ becomes constant only after $t = 50$. For $Sc = 7$ and, more especially $Sc = 15$, the magnitude of $S_\theta(t)$ continues to increase at a significant rate at the largest t. Although there is a continuous improvement in terms of resolving the smallest scalar scales as t increases, it is clear that the task of closing the integrand in the numerator of (18) becomes increasingly daunting as Sc increases. It is easy to show that the major contribution

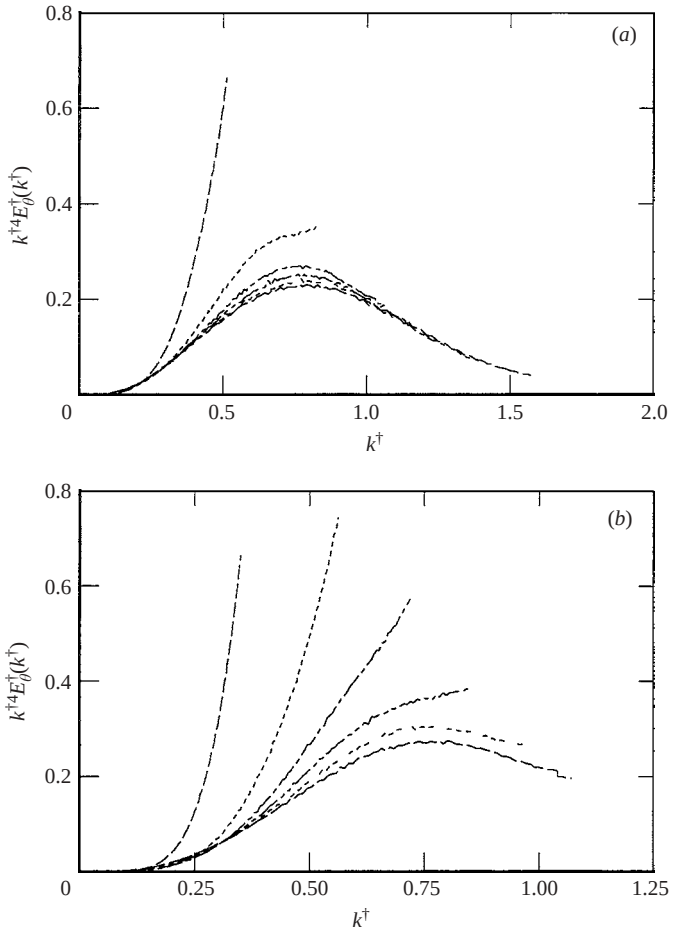

FIGURE 23. Distributions of $k^{\dagger 4}E_\theta^\dagger(k^\dagger)$ for (*a*) $Sc = 7$ and (*b*) $Sc = 15$. – –, $t = 10$; - - -, 20; — - —, 30; — - - —, 40; --- ---, 50; — —, 60.

to $\int_0^\infty k^2 T_\theta(k,t)\,\mathrm{d}k$ comes from $\int_0^\infty k^4 E_\theta(k,t)\,\mathrm{d}k$. As for $S(t)$, $S_\theta(t)$ can be regarded as receiving contributions from two terms, namely

$$S_\theta(t) = S_{\theta_1}(t) + S_{\theta_2}(t),$$

with

$$S_{\theta_1}(t) = -\frac{2}{15}\frac{\partial/\partial t\int_0^\infty k^2 E_\theta(k,t)\,\mathrm{d}k}{\left[\int_0^\infty \mathrm{k}^2 E(k,t)\,\mathrm{d}k\right]^{1/2}\left[\int_0^\infty k^2 E_\theta(k,t)\,\mathrm{d}k\right]}$$

and

$$S_{\theta_2}(t) = -\frac{4}{15}\nu_\theta\frac{\int_0^\infty k^4 E_\theta(k,t)\,\mathrm{d}k}{\left[\int_0^\infty \mathrm{k}^2 E(k,t)\,\mathrm{d}k\right]^{1/2}\left[\int_0^\infty k^2 E_\theta(k,t)\,\mathrm{d}k\right]}.$$

$S_{\theta_1}(t)$ can be rewritten, after some algebra, as

$$S_{\theta_1}(t) = -\frac{4}{15}\left(\frac{10}{3}\right)^{1/2}\frac{m-1}{n}\,R_\lambda^{-1}$$

For our 240^3 simulation, the magnitude of $S_{\theta_1}(t)$ is about 0.02 at $t=60$ (this applies over the range $0.7 \lesssim Sc \lesssim 7$). This is negligible in comparison to the values of $S_\theta(t)$ in figure 21. For $Sc=1$ (figure 22), the G92 distributions (figure 22*a*) show the same evolution with t as those in figure 20(*a*). By contrast, if the data at $t=10$ are discarded, the Batchelor-normalized distributions in figure 22(*b*) collapse well, implying that constancy with respect to t of $S_\theta(t)$ is consistent with Batchelor-similarity for small scalar scales but not with G92. For $t>20$, the closure of the distributions in figure 22 is satisfactory so that the result $S_\theta(t)=\text{const}$ cannot be in question. For $Sc=7$ (figure 23*a*) and 15 (figure 23*b*), it would be of interest to extrapolate the integrand $k^{\dagger 4}E_\theta^\dagger(k^\dagger)$ to values of $k^\dagger$ as large as 3; the Kraichnan (1968) model, which has been shown to be relevant at large $k^\dagger$ (e.g. Bogucki *et al.* 1997; Niewstadt & Brethouwer 2000; Antonia & Orlandi 2003*b*), could be used for this purpose.

7. Concluding comments

Overall, the present DNS data provide only qualified support for the equilibrium similarity, as outlined in G92. Perhaps the strongest support for G92 is reflected in the way the calculations of the transfer functions, based on G92, reproduce the DNS distributions for $T(k)$ and $T_\theta(k)$. There seems little doubt, however, that over a range of t which complies with G92, the energy spectra and transfer functions collapse better on Kolmogorov variables than with G92. Similarly, scalar spectra and transfer functions collapse better on Batchelor variables than with G92. The improved collapse is best observed at high wavenumbers, e.g. the linear–linear plots of figures 19 and 22 where high wavenumbers are emphasized. As a consequence of this, the skewness S and mixed skewness S_θ approach constant values at large t and the products SR_λ and $S_\theta R_\lambda$ are not constant, as required by G92. Unlike previous DNS data, the present 240^3 simulation adequately captures the smallest dissipative scales of motion as illustrated by the closure of the distributions in figures 19 and 22, thus permitting estimations of S and S_θ although, in the latter case, this has only been possible for $Sc \lesssim 3$. Assuming that the framework of similarity is valid, the scaling variables identified in G92 satisfy (1) and (2) rigorously. The apparent failure of the data to verify G92 at all scales of motion raises some concern. A possible inference from this is that the concept of equilibrium similarity is perhaps too rigorous in that it requires similarity to be continuously maintained between all scales of motion; this requirement may be unrealistic when, for example, the non-stationary terms in (1) and (2) become negligible and the local spectral balance at high enough wavenumbers is primarily dictated by the transfer and dissipative terms. There is no question that the concept is tenable in an asymptotic sense, when m is -1 and R_λ is constant. In this case, G92 is, as originally pointed out by George (1992*a*), fully consistent with Kolmogorov scaling. Another possibility is that there are sufficient shortcomings in both numerical and experimental data to prevent G92 from being tested properly. This should provide numericists and experimenters with sufficient incentive to continue to improve simulations and experimental realizations of decaying homogeneous isotropic turbulence.

R.A.A. and P.O. acknowledge the support of the Australian Research Council and of MURST 60%. We thank Alan Wray for making his pseudospectral code and results of his 512^3 simulations available to us and for clarifying many aspects of his simulations. We also thank Bill George for many enlightening discussions.

Appendix

In this appendix, empirical expressions for the energy and scalar transfer functions are calculated by assuming similarity based either on Kolmogorov or Batchelor variables. We also assume power-law decay rates, as given by (3) and (13). The primary motivation here is to exploit the good collapse exhibited in figures 9(*b*), 10(*b*), 11(*b*) and 12(*b*), notwithstanding the knowledge that this type of similarity does not apply at small k. The present approach differs somewhat from that in Helland *et al.* (1977) where an empirical form for $E(k)$ was used to allow the calculation of $T(k)$ to be extrapolated to relatively large R_λ. Here, the calculation is based on DNS distributions of $E^*(k^*)$.

(*a*) *Kolmogorov similarity*

We postulate that

$$E(k,t) = U_\kappa^2 \eta E^*(k^*), \tag{A 1}$$

$$T(k,t) = \left(\nu U_\kappa^2/\eta\right) T^*(k^*). \tag{A 2}$$

The scale $(\nu U_\kappa^2/\eta)$ in (A2) can be replaced by U_κ^3 since $U_\kappa \eta/\nu \equiv 1$.

Substituting the above expressions into (1) and making use of the power-law relations (3) and (4), we obtain, after some algebra,

$$T^* = 2k^{*^2} E^*(k^*) + \frac{(n-1)}{4} t^{*^{-1}} [E^*(k^*) - k^* E^{*\prime}(k^*)], \tag{A 3}$$

where the prime denotes differentiation with respect to $k*$. The appearance of $t^* \equiv (t\langle\varepsilon\rangle^{1/2}/\nu^{1/2})$ in (A3) is incompatible with the assumption that E^* and T^* depend only on k^*. This discrepancy arises from the arbitrary choice of the scales in (A1) and (A2). These scales are, however, consistent with a t^{-1} decay of $\langle q^2(t)\rangle$ and with $R_\lambda = \text{constant}$.

(*b*) *Batchelor similarity*

Here we assume that

$$E_\theta(k,t) = \theta_B^2 \eta_B E_\theta^\dagger(k^\dagger),$$

$$T_\theta(k,t) = \theta_B^2 \eta_B \gamma\, T_\theta^\dagger(k^\dagger).$$

The above expressions are substituted into (2) and use is made of the power-law relations for (3), (4), (13), (14). After some algebra, the final result is

$$T_\theta^\dagger(k^\dagger) = \left(2k^{\dagger^2} + \left(m - \frac{3n}{4} - \frac{1}{4}\right) t^{*^{-1}}\right) E_\theta^\dagger(k^\dagger) - (n-1) t^{*^{-1}} k^\dagger E_\theta^{\dagger\prime}(k^\dagger), \tag{A 4}$$

where the prime here denotes differentiation with $k^\dagger$. Note that unlike (15), (A 4) contains a dependence on both m and n.

REFERENCES

Antonia, R. A. & Orlandi, P. 2003*a* Effect of Schmidt number on small-scale passive scalar turbulence. *Appl. Mech. Rev.* **56**, 615–632.

Antonia, R. A. & Orlandi, P. 2003*b* On the Batchelor constant in decaying isotropic turbulence, *Phys. Fluids* **15**, 2084–2086.

Antonia, R. A., Smalley, R. J., Zhou, T., Anselmet, F. & Danaila, L. 2003 Similarity of energy structure functions in decaying homogeneous isotropic turbulence. *J. Fluid Mech.* **487**, 245–269.

Batchelor, G. K. 1948 Energy decay and self-preserving correlation functions in isotropic turbulence. *Q. Appl. Maths* **6**, 97–116.

Batchelor, G. K. & Townsend, A. A. 1948 Decay of isotropic turbulence in the initial period. *Proc. R. Soc. Lond.* A **193**, 539–558.

Bogucki, D., Domaradzki, J. A. & Yeung, P. K. 1997 Direct numerical simulations of passive scalars with $Pr > 1$ advected by turbulent flow. *J. Fluid Mech.* **343**, 111–130.

Brethouwer, G. & Niewstadt, F. T. M. 1999 Mixing of weakly and strongly diffusive scalars in isotropic turbulence in direct and large-eddy simulation III. *Proc. Isaac Newton Institute Symposium/EROFTAC Workshop, Cambridge.*

de Bruyn Kops, S. M. & Riley, J. J. 1998 Direct numerical simulation of laboratory experiments in isotropic turbulence. *Phys. Fluids* **10**, 2125–2127.

Comte-Bellot, G. & Corrsin, S. 1966 The use of a contraction to improve the isotropy of grid-generated turbulence. *J. Fluid Mech.* **25**, 657–682.

Comte-Bellot, G. & Corrsin, S. 1971 Simple Eulerian time correlation of full and narrow band velocity signals in grid-generated 'isotropic' turbulence. *J. Fluid Mech.* **48**, 273–337.

Domaradzki, A. & Rogallo, R. S. 1990 Local energy transfer and non local interactions in homogeneous, isotropic turbulence. *Phys. Fluids* A **2**, 413–426.

Dryden, H. L. 1943 A review of the statistical theory of turbulence. *Q. Appl. Maths* **1**, 7–42.

George, W. K. 1992*a* The decay of homogeneous isotropic turbulence. *Phys. Fluids* A **4**, 1492–1509.

George, W. K. 1922*b* Self-preservation of temperature fluctuations in isotropic turbulence. In *Studies in Turbulence* (ed. T. B. Gatskii, S. Sarkar & G. Speziale), pp. 514–528. Springer.

George, W. K. & Wang, H. 2002 The spectral transfer in isotropic turbulence. *Proc. Princeton IUTAM High Re Flow Meeting, Sept 2002* (to appear).

Goldstein, S. 1951 On the law of decay of homogeneous isotropic turbulence and the theories of the equilibrium and similarity spectra. *Proc. Camb. Phil. Soc.* **47**, 554–574.

Gotoh, T., Fukayama, D. & Nakano, T. 2002 Velocity field statistics in homogeneous steady turbulence obtained using a high resolution DNS. *Phys. Fluids* **14**, 1065–1087.

Helland, K. N., Van Atta, C. W. & Stegen, G. R. 1977 Spectral energy transfer in high Reynolds number turbulence. *J. Fluid Mech.* **79**, 337–359.

Kaneda, Y., Ishihara, T., Yokokawa, M., Itakura, K. & Uno, A. 2003 Energy dissipation rate and energy spectrum in high resolution direct numerical simulations of turbulence in a periodic box. *Phys. Fluids* **15**, L21–L24.

von Kármán, T. & Howarth, L. 1938 On the statistical theory of isotropic turbulence. *Proc. R. Soc. Lond.* A **164**, 192–215.

von Kármán, T. & Lin, C. C. 1949 On the concept of similarity in the theory of isotropic turbulence. *Rev. Mod. Phys.* **21**, 516–519.

Kerr, R. M. 1985 Higher-order derivative correlations and the alignment of structures in isotropic numerical turbulence. *J. Fluid Mech.* **153**, 31–58.

Kerr, R. M. 1990 Velocity, scalar and transfer spectra in numerical turbulence. *J. Fluid Mech.* **211**, 309–332.

Kim, J. & Antonia, R. A. 1993 Isotropy of the small scales of turbulence at low Reynolds number. *J. Fluid Mech.* **251**, 219–238.

Kolmogorov, A. N. 1941 The local structure of turbulence in an incompressible fluid for very large Reynolds numbers. *Dokl. Akad. Nauk. SSSR* **30**, 299–303.

Kolmogorov, A. N. 1962 A refinement of previous hypotheses concerning the local structure of turbulence in a viscous incompressible fluid at high Reynolds number. *J. Fluid Mech.* **13**, 82–85.

Kraichnan, R. 1968 Small-scale structure of a scalar field convected by turbulence. *Phys. Fluids* **11**, 945–953.

Lin, C. C. 1948 Note on the law of decay of isotropic turbulence. *Proc. Natl Acad. Sci.* **34**, 540–543.

Mansour, N. N. & Wray, A. A. 1994 Decay of isotropic turbulence at low Reynolds number. *Phys. Fluids* **6**, 808–814.

Mydlarski, L. & Warhaft, Z. 1996 On the onset of high-Reynolds-number grid-generated wind tunnel turbulence. *J. Fluid Mech.* **320**, 331–368.

Mydlarski, L. & Warhaft, Z. 1998 Passive scallar statistics in high-Peclet-number grid turbulence. *J. Fluid Mech.* **358**, 133–175.

Nelkin, M. 1994 Universality and scaling in fully developed turbulence. *Adv. Phys.* **43**, 143–181.

Nieuwstadt, F. T. M. & Brethouwer, G. 2000 Turbulent transport and mixing. In *Advances in Turbulence VIII* (ed. C. Dopazo *et al.*) pp. 133–140. CIMNE, Barcelona.

Orlandi, P. 1999 *Fluid Flow Phenomena, A Numerical Tool Kit*. Kluwer.

Orlandi, P. & Antonia, R. A. 2002 Dependence of the non-stationary form of Yaglom's equation on the Schmidt number. *J. Fluid Mech.* **451**, 99–108.

Speziale, C. G. & Bernard, P. S. 1992 The energy decay in self-preserving isotropic turbulence revisited. *J. Fluid Mech.* **241**, 645–667.

Uberoi, M. S. 1963 Energy transfer in isotropic turbulence. *Phys. Fluids* **6,** 1048–1056.

Van Atta, C. W. & Chen, W. Y. 1969 Measurements of spectral energy transfer in grid turbulence. *J. Fluid Mech.* **38**, 743–763.

Wang, H. & George, W. K. 2002 The integral scale in homogeneous isotropic turbulence. *J. Fluid Mech.* **459**, 429–443.

Wang, H., Sonnenmeier, J. R., Gamard, S. & George, W. K. 2000 Evaluating DNS simulations of isotropic decaying turbulence using similarity theory. *ICTAM Symp., Chicago, 27 August–2 September, 2000.*

Warhaft, Z. & Lumley, J. L. 1978 An experimental study of the decay of temperature fluctuations in grid-generated turbulence. *J. Fluid Mech.* **88**, 659–684.

Wray, A. 1998 Decaying isotropic turbulence. In *AGARD Advisory Report*, vol. **345**, pp. 63–64.

Yeh, T. T. & Van Atta, C. W. 1973 Spectral transfer of scalar and velocity fields in heated grid turbulence. *J. Fluid Mech.* **58**, 233–261.

Yeung, P. K., Xu, S. & Sreenivasan, K. R. 2002 Schmidt number effects on turbulent transport with uniform mean scalar gradient. *Phys. Fluids* **14**, 4178–4191.

Zhou, T., Antonia, R. A., Danaila, L. & Anselmet, F. A. 2000 Transport equations for the mean energy and temperature dissipation rates in grid turbulence. *Exps. Fluids* **28**, 143–153.